THIRTY METER TELESCOPE

TMT SITE TESTING FINAL REPORT

TMT.SIT.TEC.08.003.REL01

Date of this release: April 8, 2008

Prepared by the **TMT Site Selection Team**

TMT CONFIDENTIAL
DO NOT DISTRIBUTE

Contributors

TMT Site Selection Team

Bob Blum, CTIO (now AURA New Initiatives Office)
Edison Bustos, CTIO
Sebastian Els, CTIO
Paul Gillett, TMT
Brooke Gregory, CTIO
Jerry Nelson, University of California, Santa Cruz
Angel Otárola, TMT
Reed Riddle, TMT
Matthias Schöck, TMT
Juan Seguel, CTIO
Warren Skidmore, TMT
Eric Steinbring, Herzberg Institute of Astrophysics
Tony Travouillon, TMT
Joselino Vasquez, CTIO
Konstantinos Vogiatzis, TMT
David Walker, CTIO
Lianqi Wang, TMT

TMT Sites Advisory Group

George Djorgovski, Caltech (Chair)
Alistair Walker, CTIO (Chair)
Gary Chanan, University of California, Irvine
Dave De Young, AURA New Initiatives Office
James Graham, University of California, Berkeley
Derek Salmon, Canada France Hawaii Telescope
Matthias Schöck, TMT
Eric Steinbring, Herzberg Institute of Astrophysics

Other contributors

The TMT site selection work could not have happened without the contributions of many other people at various institutions. A special thanks to everybody who has supported, and is still supporting, the TMT site selection program, in particular the people at the Cerro Tololo Inter-American Observatory (CTIO), the National Optical Astronomy Observatory (NOAO) and the AURA New Initiatives Office (NIO), the Universidad Católica del Norte in Antofagasta, the Observatorio Astronómico Nacional de San Pedro Mártir, Gemini Observatory, Palomar Observatory, the Submillimeter Array (SMA), the University of Hawaii Institute for Astronomy (IfA), the University of Lethbridge, the University of Moscow, the South African Astronomical Observatory (SAAO), and the entire TMT project including its partner institutions and external reviewers.

Contents

1 Purpose of this Report

The TMT Site Testing Final Report provides information about atmospheric and other environmental properties of the TMT candidate sites. The TMT Project is planning to make a down-select to one northern hemisphere and one southern hemisphere site based on this information as well as on observatory technical and programmatic considerations. The final site selection will also be based on this report, augmented by other technical and programmatic information gained after the release of this report.

This report provides high-level information about the site selection process, the instrumentation and the results from the candidate sites. Detailed information about the different aspects of the site selection process are given in the supplementary documents listed in Section 8.

2 The TMT Site Selection Process

TMT needs to be built on the best available site in order to obtain the maximum return from its science potential. Careful site selection has therefore been extremely important to TMT from the very beginning of the project. The site selection process started in 2001/2002, in a collaboration between the AURA New Initiatives Office (NIO) and the California Extremely Large Telescope (CELT), with the pre-selection of five[1] candidate sites to be studied in detail. On-site testing via the operation of remote site monitoring stations has been in progress since 2003 and will continue until the review of this report, after which testing on most of the candidate sites will likely be discontinued.

The selection of the TMT site depends on a multitude of parameters, both technical and non-technical, and it is not a priori obvious how to combine these parameters to arrive at the final site decision. A series of steps have therefore been taken by the TMT Project to develop a method of dealing with the complexity of the TMT site selection process. These include quarterly reviews of the site selection process and data, quarterly results update reports, presentations of site results at TMT SAC and other project meetings, as well as the issuing of intermediate reports such as the Site Selection Intermediate Report (1 July 2006) and the Site Qualification Report (1 July 2007). The Site Selection Process was also reviewed by the External Advisory Panel (EAP) at the TMT Construction Proposal Review (June 2007) and will be reviewed again at the EAP Review in June 2008.

These steps serve the purpose of providing information to the parties involved in the site decision and of fine-tuning our data analysis and site comparison methodology. The final step of the official site testing period is the issuing of the Site Selection Final Report (this report), which will first undergo an internal review on April 22, 2008. On April 28, 2008, the Project Manager will present a recommendation to the TMT Board, which will then make a down select to a northern hemisphere and a southern hemisphere site. The EAP will review the report, the results from the sites and the site selection process in June 2008.

[1] Originally, six candidate sites were selected. One of them was dropped from the list before deployment of site testing equipment. See Section 4.

3 TMT Site Selection Requirements

The TMT site needs to be suited for producing astronomical data of superb quality and for building and operating an observatory of the size and complexity of TMT. Strict technical requirements as they apply to other parts of the project do not exist for the TMT site, as there are no hard cut-offs for the parameters entering the TMT site decision beyond which a site becomes unsuitable. Instead, the site selection process involves measuring and predicting both the technical and programmatic properties of the sites and balancing them so as to determine the site that best meets the TMT needs. The process employs a site ranking metric which provides a method for an objective comparison of the technical properties of the candidate sites and their science producing implications.

This section provides a brief summary of the TMT site selection requirements. Details are given in the Site Selection Requirements and Strategy Document (SiRD), the Science-Based Requirements Document (SRD) and the Observatory Requirements Document (ORD). Details of the site ranking metric are given in the TMT Site Merit Function report.

3.1 Science-Based Requirements and Site Astronomical Criteria

The TMT site is required to enable maximum use of TMT as a facility planned to operate in the 0.3 to 30 μm wavelength range with adaptive optics as an integral element in achieving the specified performance. One of the most important properties of a qualified site is a high percentage of time on the sky with favorable combinations of factors such as absence of clouds, good seeing and low precipitable water vapor. Section 2.2 of the Science-Based Requirements Document (SRD) lists key features:

Key astronomical features:
- High fraction of clear nights
- Excellent image quality (large r_0)
- Large isoplanatic angle, θ_0
- Long turbulence coherence time, τ_0
- Small outer scale, L_0
- Large fraction of the non-photometric nights should be spectroscopic
- Low precipitable water vapor
- Low typical temperatures
- High altitude

Other performance related features:
- Low wind speed distribution to limit telescope buffeting (but sufficiently high to enable enclosure flushing)
- Minimal change of temperature during the night
- Minimal seasonal temperature variations
- Minimal day-night temperature variations
- Latitude (for overlap with key observatories such as ALMA)

Cost related features:
- Easy physical access for minimizing construction costs
- Good human access for minimizing operating costs
- Availability of site

Other engineering / safety features:
- High mechanical integrity of soil
- Low seismicity

Flowing from the science-based requirements, a list of site astronomical criteria was developed that will enter the site decision. The astronomical parameters to be considered are described in Section 5 of the SiRD, together with the criteria and goals for site characteristics and measurements. The kind of results to be produced during the site selection process are also described there. The range of potentially important site characteristics includes:

Weather-related characteristics:
- Cloud cover
- Photometric conditions
- Low-elevation wind (below 800m)
- High-elevation wind (800m and above; not measured)
- Temperature
- Ground-level humidity
- Precipitable water vapor

Turbulence-related characteristics:
- Overall seeing
- Turbulence profiles
- Isoplanatic angle
- Turbulence time constant
- Outer scale of turbulence (not measured)

Other characteristics:
- Low-elevation dust
- High-elevation dust (not measured)
- Light pollution
- Atmospheric transparency (not measured quantitatively)
- Sky brightness (not measured)
- Sodium layer properties (not measured)

Note that not all of these parameters are measured during the TMT site selection process (as indicated above) as this would have been beyond the means of the project. The methods and instrumentation used to assess these site characteristics are described in Sections 5 and 6 of this report. The results are summarized in Section 7 and are presented in detail in the TMT Site Selection Results Update and the 30 m Tower Results Update, which are provided together with this report.

3.2 Observatory Technical and Programmatic Requirements

In addition to being scientifically qualified, the TMT site must also meet observatory technical and programmatic needs. Obtaining legal possession and access to the site when required in the construction schedule is a primary factor, but other considerations such as labor, logistics, geological conditions and the permitting process will also be considered in the site selection. These aspects are summarized in Table 1 and are described in Sections 3 and 6 of the SiRD. They are not addressed in this report.

3.3 Other Requirements

A list of specific, site-dependent requirements for design, construction and operation of the observatory are given in Section 3.1 of the Observatory Requirements Document (ORD). These include

Issue	Method
Construction and operating cost and method	TMT cost estimate
Cultural, environmental and land use issues	Consultations with local groups; archaeological, fauna and flora studies; assessment of historical preservation and environmental issues
Labor force issues	Evaluation of labor supply, skill level, local conditions
Proximity to astronomers and astronomy infrastructure	Evaluation of existing observatories, organizations
Geological and geotechnical conditions	Geological and geotechnical studies
Foundation conditions	Evaluation of telescope pier and enclosure foundations
Vibration transmission	Evaluation of the vibration transmission through the soil from the enclosure and other equipment to the telescope structure
Compatibility with surrounding area	Studies of conditions and how TMT will fit in
Economic impact of siting TMT	Study of TMT's impact
Permitting, land ownership etc.	Negotiations with local authorities
Transportation	Evaluation of local situation
Customs and immigration issues	Evaluation of applicable regulations

Table 1: Other aspects entering the TMT site decision. These issues are not described in this document.

performance, operating and survival conditions for temperature, wind, humidity, precipitation, lightning and earthquakes. Section 4 of the ORD shows the standard atmosphere model used by TMT until the final site has been selected.

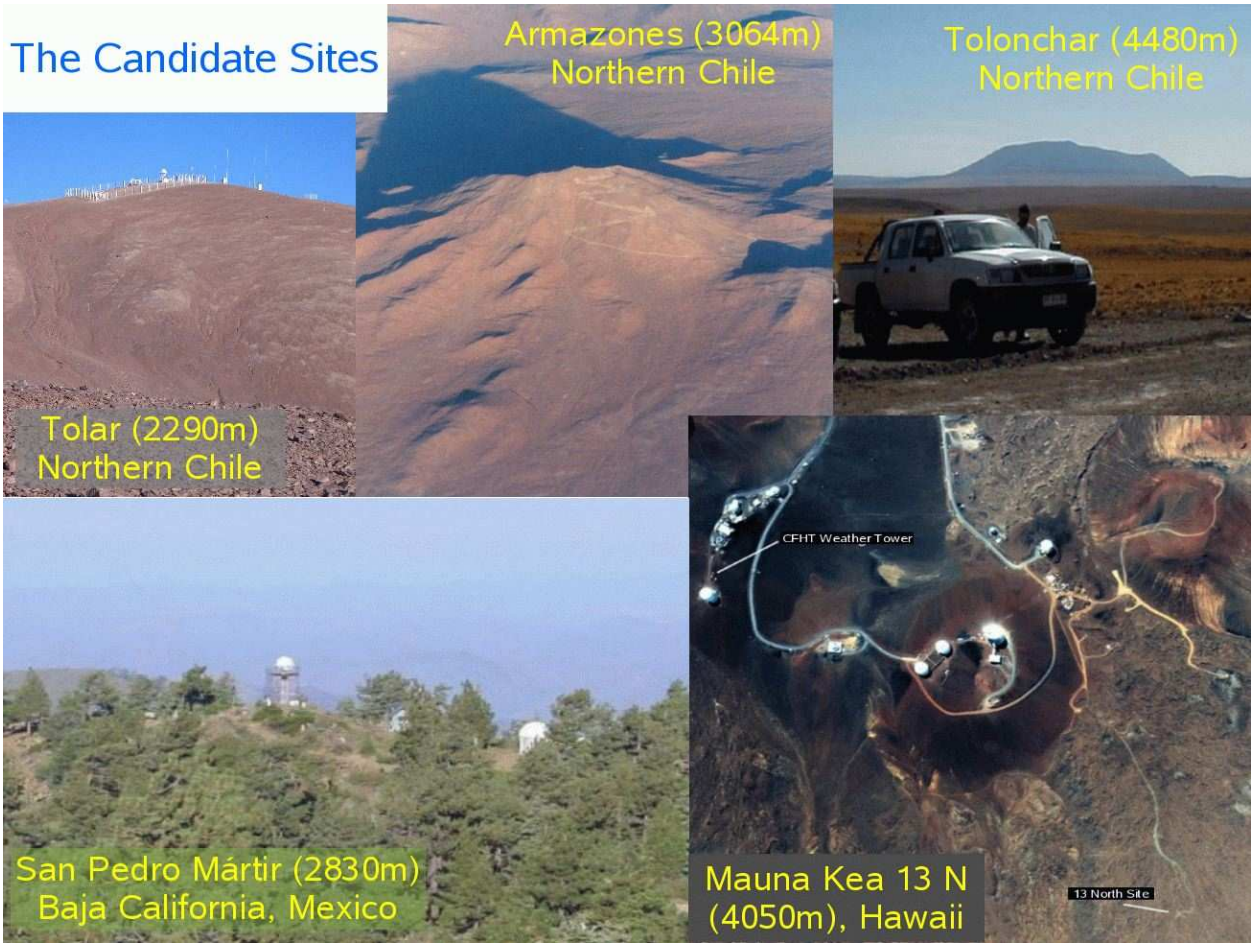

Figure 1: Views of the five TMT candidate sites.

4 Candidate Sites

TMT selected six sites as candidate observatory sites and began on-site testing in 2003 (see Table 3 in Section 5 for details of the instrument deployment schedule). The site selection process started by considering as complete a list as possible of potentially interesting sites everywhere in the world. It was narrowed down using existing knowledge from previous site selection studies and from established observatory sites. The final list of candidate sites was selected based on satellite studies of cloud cover and precipitable water vapor done by Dr. D.A. Erasmus. The details of the candidate site selection are given in Section 8 of the SiRD.

No equipment was installed on one of these sites, Cerro Quimal near Calama in northern Chile, as our petition for a permit to deploy the site testing equipment was denied. The names of the remaining five candidate sites and their coordinates, along with some of the main results from the satellite studies, are listed in Table 2. Views of each of the candidate sites are shown in Fig. 1. General descriptions of the sites and their locations are given in the following. Results from the on-site characterization are presented in Section 7.

Site Name	Elevation	Latitude [deg N]	Longitude [deg W]	Clear / Usable Cloud Fraction	Median / 10% PWV [mm]
Cerro Tolar	2290 m	-21.9639	70.0997	81% / 85%	4.02 / 1.59
Cerro Armazones	3064 m	-24.5800	70.1833	80% / 86%	2.87 / 1.15
Cerro Tolonchar	4480 m	-23.9333	67.9750	70% / 78%	1.70 / 0.70
San Pedro Mártir	2830 m	31.0456	115.4691	73% / 80%	2.63 / 1.06
Mauna Kea 13N	4050 m	19.8330	155.4810	69% / 78%	1.86 / 0.72

Table 2: List of TMT candidate sites selected for on-site testing. Besides the coordinates, the clear and usable cloud fraction and the median and best ten percentile precipitable water vapor (PWV) values are given. The values shown are those used for the selection of the candidate sites and were determined in the Erasmus satellite data studies. They differ slightly from the values given in Section 7.

4.1 Cerro Tolar

A low elevation site (2290 m) in northern Chile, Cerro Tolar is in the Atacama desert and has an extremely arid climate. Tolar is located at a distance of only 8 km from the coast, at 16 km from the closest paved road and 18 km north-north-east of Tocopilla, a town of 25,000 inhabitants. [Note: All distances given in this section are straight line distances. Driving distance are usually 50–100% longer.] The closest commercial port, airport and major population center is Antofagasta (population 225,000), 190 km south of Tolar. There is a primitive four-wheel drive road to the summit, where some radio equipment is installed.

The summit area is small and a significant amount of earth would have to be moved to accommodate TMT. We are not aware of Tolar having any cultural or archaeological significance to the local people.

In spite of its closeness to Tocopilla, light pollution is not an issue, as the bluffs above Tocopilla are ∼1000 m high and block most of the light produced in town, but some glow from town is visible nevertheless. Some small light sources from mines are visible in the south and south-east.

Testing of Tolar was stopped in April 2007 because parts of the solar power system were needed to support an augmented site testing effort on Cerro Armazones and Cerro Tolonchar. At the time, Tolar was the site for which we had the longest time series of data. Because only small seasonal and annual variations were observed in the four years of testing on Tolar and because Armazones and Tolonchar were deemed more likely candidates for the TMT site, it was judged more important to augment testing on Armazones and Tolonchar than to continue on Tolar.

4.2 Cerro Armazones

Cerro Armazones, a medium elevation site (3064 m) in northern Chile, is also located in the Atacama desert and close to the coast (36 km), with a climate very similar to that of Tolar. It is 22 km from ESO's Very Large Telescope (VLT) on Cerro Paranal and 110 km south of Antofagasta, the closest city. A good, but steep and narrow switch-back road to the summit exists. The closest paved road is ∼18 km from Armazones, connected by a rough dirt road.

Armazones is the site of a small observatory operated by the Universidad Católica del Norte in Antofagasta. This observatory is not located on the summit, but on a saddle ∼350 m below the summit. A new observatory utilizing a hexapod mounted telescope is being commissioned by the University Bochum on Cerro Murphy, a small peak 1.5 km south-west of Armazones and ∼225 m

lower.

The summit area is small, albeit somewhat larger than that of Tolar, requiring leveling down to ∼11 m below the current high point for TMT to be built on Armazones. No cultural or archaeological significance of Armazones is known. An archaeological study of the mountain found no artifacts.

The only lights visible from Armazones are glows close to the horizon from Antofagasta in the north-north-east and from the large, albeit distant Mina Escondida (120 km to the east-north-east). Some prospecting is going on in the area and needs to be monitored.

4.3 Cerro Tolonchar

Cerro Tolonchar is the eastern-most of the Chilean sites, south of the Salar de Atacama, and only 25–80 km from several 5000–6000 m peaks of the Andes. Because of its eastern location and higher altitude, it experiences more precipitation and clouds than Tolar and Armazones, especially during the "Bolivian Winter" from approximately mid December to mid February. Tolonchar is also the highest (4480 m) and most remote of all TMT candidate sites. The closest settlement is Socaire (300 inhabitants) 38 km to the north, with the closest towns being Toconao (550 inhabitants) at 80 km, San Pedro de Atacama (an eco-tourism town of 1,500 people) at 115 km and Calama, the next large city with a commercial airport (120,000 inhabitants), at 190 km. The driving time is currently 2 h from Socaire, 3 h from San Pedro de Atacama and 4.5 h from Calama. Antofagasta, 250 km distant, can be reached via a different route in ∼5.5 h. These times can be reduced by 30–60 min through the construction of a good road to Tolonchar. Currently, only a rough 4WD road exists from the Paso Sico road to the base of Tolonchar (closest distance ∼17 km). TMT has constructed a road from the base to the summit which is designed to be usable, with some improvements, for the observatory should TMT be built there.

The summit area is large and flat and would require little work to accommodate TMT. There is a stone structure of cultural significance on the summit and some artifacts were found, and carefully avoided, during the road construction. Given the size of the summit area, it should be possible to avoid any such structure even for a building the size of TMT. Tolonchar has some significance to the local people. This is under investigation.

Some lights of mines in and around the Salar de Atacama, approximately 50 km distant but with a direct line of sight, from the Mina Escondida and from the towns described above are visible close to the horizon, but Tolonchar remains a very dark site.

4.4 San Pedro Mártir

San Pedro Mártir (SPM) is located in northern Baja California, Mexico, inside a national park and is the site of the Observatorio Astronómico Nacional de San Pedro Mártir. It is a medium-elevation site (2830 m), ∼65 km from the Pacific coast in the west and 55 km from the Sea of Cortez (Gulf of California) to the east. The terrain is gently rising from the north, west and south, with a steep cliff dropping more than 2000 m to the desert in the east. The highest point of the area and, in fact, of Baja California, Picacho del Diablo (3095 m), is approximately 6 km to the south-east of the observatory. The area is inside a pine forest and receives more precipitation than the other TMT candidate sites, although most of that comes down in a number of strong events with mostly clear time in between. The closest town is Ensenada (300,000 inhabitants) at 4 h driving time and 140 km line-of-sight distance. The closest commercial airports are in Tijuana (at 220 km) and San Diego (250 km).

There is an existing road all the way to the observatory. It is paved to the national park

entrance, ∼20 km from the observatory, after which it would have to be improved if TMT selected San Pedro Mártir. Some work in the summit area, potentially involving moving one of the existing telescopes, would be required to accommodate TMT.

The surrounding area is very dark from the north-east through the south to the west. In northern directions, the San Diego/Tijuana and Mexicali/Yuma (180/200 km) areas and Ensenada in the north-west produce visible glows, but due to their distance, San Pedro Mártir remains a very dark site.

4.5 Mauna Kea 13N

The TMT candidate site on Mauna Kea on the Big Island of Hawaii is a location referred to as "13 North" (13N) on the northern shield, approximately 150 m below the summit. It is adjacent to the Submillimeter Array (SMA) extension area. With ∼4050 m elevation, 13N is the second highest of the TMT candidate sites. The conditions are usually dominated by a stable north-easterly flow, but can produce severe weather and precipitation, in particular in the winter. As a developed site with several observatories, much of the infrastructure required for TMT exists on Mauna Kea. Only a short piece of road would have to be constructed to the 13N site. The 13N area is relatively flat, but some earth moving would be required nevertheless due to its location inside a somewhat sloping lava field.

Mauna Kea is of great cultural and archaeological significance to the local people. What effect this has on the potential construction of TMT at 13N is currently under investigation.

The lights from most of the towns in the north and west of the Big Island are visible from the 13N location, as well as the glow from Hilo. However, as for all the other sites, the vertical extent of the light pollution remains well below the 65 degree zenith angle observing limit of TMT [see Section 6.6.3, *Riddle08* and *Schöck08c*].

Figure 2: The TMT site selection instrument suite.

5 The TMT Site Selection Instrument Suite

The TMT site decision will be based on both technical and programmatic aspects. Technical site properties are assessed predominantly through data acquired in a multi-year study of the site conditions using identical equipment. To acquire these data, the TMT site testing team has been operating remote site monitoring stations at each of the candidate sites. Considerable effort has gone into calibrating all equipment through side-by-side comparisons of identical instruments and, when possible, by comparison with other instruments. This section contains a summary of the instrument suite, the deployment dates to the sites and the measurement uncertainties we have determined for the individual parameters. Details about each of the instruments are given in Section 6.

5.1 Instrument Overview

The following instruments have been deployed at the candidate sites (see also Fig. 2):

- **Differential Image Motion Monitors (DIMM):** The TMT DIMMs are mounted on small (35cm) but robust custom-made telescopes installed on 6.5 m towers. A DIMM measures the integrated seeing in the air column above the telescope.

- **Multi-Aperture Scintillation Sensors (MASS):** Scintillation-based instruments which measure 6-layer turbulence profiles, the isoplanatic angle and the turbulence coherence time. Can also be used for atmospheric transparency estimates.

- **Sound Detection and Ranging (SODAR) acoustic sounders:** Phased-array acoustic emitter/receiver systems which produce low elevation (10 – 800 m) turbulence and wind profiles.

- **Automatic Weather Stations (AWS):** Commercial weather stations with temperature (air and soil), wind speed and direction, humidity, barometric pressure, precipitation, solar irradiation, heat flux and net radiation sensors. Stand-alone units mounted $\sim$2 m above the ground. Air temperature sensors are also installed on 30 m towers on Armazones and Tolonchar.

- **Sonic Anemometers:** Mounted at the MASS/DIMM telescope level and/or at several elevations on the 30 m towers. Measure wind speed and direction, an approximate temperature value, and can be used to estimate the in-situ turbulence strength. [During their site survey, the Large Synoptic Survey Telescope (LSST) project also had a 30 m tower with sonic anemometers installed at San Pedro Mártir. The data from this are available to us.]

- **All-sky cameras (ASCA):** Provide images of the entire sky in several visible and infrared filters. Used for cloud analyses and light pollution studies.

- **Infrared Radiometers for Millimetre Astronomy (IRMA):** Measure the flux from the sky at 20 μm. The precipitable water vapor (PWV) content of the atmosphere can be calculated from this using a suitable atmospheric model.

- **Dust Sensors:** Commercial particle counters mounted at the MASS/DIMM telescope level. Measure the particle density in five different channels for particle sizes of 0.3, 0.5, 1.0, 2.0 and 5.0 μm.

In addition to the on-site testing, other methods used to characterize the sites are:

- **Computational Fluid Dynamics (CFD) Simulations:** Used to verify results obtained at the candidate sites, to assess the impact of site preparation and construction, and to evaluate dome/mirror seeing and wind shake.

- **Satellite Studies of Cloud Cover and PWV:** Based on meteorological satellite data studies carried out by Dr. D. A. Erasmus and his group. Used for the pre-selection of candidate sites and to put the on-site data into the perspective of a longer temporal baseline.

5.2 Instrument Deployment Schedule

The original goal of the TMT site selection campaign was to take on-site measurements of all major parameters (e.g. weather, seeing) for at least 2 years, and for at least one year for all other parameters. This was achieved or exceeded for most instruments, but was not possible in all cases for practical reasons. Dates of the first deployments of all instruments are shown in Table 3. Note that we do not have five sets of all instruments, so that not all of them have been installed continuously at each site since the dates given in the table. Also, data taken soon after the first

	Tolar	Armazones	Tolonchar	San Pedro Mártir	Mauna Kea 13N
Weather station	Apr 03	Jul 03	Nov 05	Oct 04	Jun 05
DIMM	Oct 03	Nov 04	Nov 05	Oct 04	Jun 05
MASS	Jan 04	Nov 04	Jan 06	Oct 04	Jul 05
SODAR	—	Mar 05	Feb 06	Mar 06	Oct 05
All-sky camera	Oct 05	Oct 05	Nov 05	Jul 05	Jun 06
Sonic anemom.	Feb 06	Feb 06	Mar 06	May 06	Nov 05
Dust sensor	Feb 06	Feb 06	Mar 06	May 06	Nov 05
30 m tower	—	Sep 06	Mar 07	Dec 05	—
IRMA	—	Jan 07	Mar 07	—	Feb 07

Table 3: Dates of first data acquisitions of the different instruments for each candidate site. Note that we only have three sets of SODARs and three IRMAs, which are rotated among the sites. Also note that the 30 m tower on San Pedro Mártir was set up and operated by the LSST project from December 2005 to May 2006. Testing on Tolar was discontinued in April 2007.

deployment dates are not as reliable in some cases as later data and might not be included in the results shown in Section 7. Details about the individual instruments are given in Section 6.

The site data are put into context of longer-term data sets (Erasmus satellite studies; data from existing observatories) as much as possible, as well as by Computational Fluid Dynamics (CFD) simulations, to investigate whether there is reason to believe that the on-site testing periods were non-representative for any of the sites.

5.3 Instrument Calibrations and Results Verifications

Data taken with our instruments are only considered useful for the TMT site selection process if the reliability and uncertainties of the measurements are known. As a result, we have gone through great efforts to understand all instruments and results, including:

- Side-by-side comparisons of identical instruments
- Side-by-side comparisons of different instruments measuring the same parameters
- Sensitivity analyses of the dependence of the results on input parameters
- Independent verification of all in-house analysis software by at least two people
- Independent verification of all results and statistics by at least two people

Details on the calibrations of the different instruments and validations of the results are given in Section 6. Here, we only present the summary of the uncertainties expected for our instruments (see Table 4). All values given in the table are limits for the statistical properties of the parameters, not for the individual measurements.

A note concerning terminology: We use the term 'absolute error' of a measurement to describe the *accuracy* of the measurement (defined as the closeness of agreement between the average value obtained from a large series of test results and an accepted reference value). It describes how well our measurements agree with the absolute values of the respective parameters (the "truth"). The term 'relative error' is used to describe the expected relative differences between the measurements taken

	Relative Error	Absolute Error	Comments
Weather station sensors			
Temperature	$\lesssim 1^\circ$C	$\lesssim 1^\circ$C	
Temperature on 30 m tower	0.1°C	0.1°C	
Wind speed	10%	10%	
Wind direction	$\lesssim 5^\circ$	$\lesssim 5^\circ$	limited by setup accuracy
Humidity	10%	10%	non-linear in mid range (around 30%)
Pressure	1 hPa	1 hPa	vendor quoted accuracy
Solar irradiance	n/a	n/a	not needed
Precipitation	n/a	n/a	used for equipment safety only
Heat flux	5%	5%	vendor quoted accuracy
Net radiation	3%	3%	vendor quoted accuracy
DIMM			
Seeing	$0\farcs02$	similar	
MASS			
Free-atmosphere seeing	$0\farcs05$	similar	
Individual layers ($C_n^2 \mathrm{d}h$)	10^{-14} m$^{1/3}$	similar	
Isoplanatic angle	$0\farcs02$	$< 0\farcs2$	
Coherence time	20%	20%	
SODAR			
Wind profiles	20%	~ 1 m/s	offsets exist between SFAS and XFAS
GL seeing	10%	similar	
Individual layers	$\sim 20\%$	similar	
Sonic anemometer			
Wind speed	$< 5\%$	$< 5\%$	
Wind direction	$\lesssim 5^\circ$	$\lesssim 5^\circ$	limited by setup accuracy
Sonic temperature	$< 3^\circ$C	$< 3^\circ$C	offsets exist
Dust sensor			
Particle count	10%	n/a	
All-sky camera			
Cloud cover	1–4%	1–4%	site dependent
IRMA			
Precipitable water vapor	~ 0.25 mm	n/a	additive offsets exist; site dependent
Satellite data			
Cloud cover	2–6%	2–6%	site dependent
Precipitable water vapor	20%	20%	

Table 4: Summary of the measurement uncertainties as determined from the instrument calibrations. Here, 'n/a' stands for 'not available'. Values given are usually upper limits to the uncertainties of the probability distributions of the respective quantities, although some exceptions apply. See Section 6 for explanations.

with identical equipment at different sites, the *reproducibility*. Both accuracy and reproducibility are difficult to determine in practice. For our results, they are based on the comparison of different equipment at the same sites, whenever possible. When this is not possible, we estimate them based on investigations of the *repeatability* of the measurements (the expected relative differences between the measurements taken with identical equipment at the same site) and on sensitivity and bias analyses of the instruments.

Also note that some of the calibrations are performed either periodically, such as every time a site is visited, or at least once at the beginning and once at the end of the site testing program. In this way, it is possible to determine whether calibrations stay constant or if drifts or jumps in time need to be accounted for. Details are presented in the site calibration reports for the individual

instruments, which are provided as supplementary information (see Section 8).

6 Instrument Details

This section provides details about the TMT site selection instrument suite. For each instrument, we present a brief description of the instrument and the parameters it measures. We describe the calibrations we have performed and the resulting conclusions concerning the uncertainties of the measurements. If care needs to be taken in the interpretation of the results, that is also described here. Detailed reports on the tests, calibrations and validations for each instrument are provided as supplementary information and are referenced in the respective sections.

6.1 Automatic Weather Stations (AWS) and Sonic Anemometers

Commercial automatic weather stations (AWSs) from Monitor Sensors are deployed at all sites. These measure air temperature, wind speed and direction, relative humidity, barometric pressure, solar irradiance and the occurrence of precipitation. The net radiation above the ground and the ground heat flux are also measured whenever a SODAR is running at a site. Soil temperature sensors have been used at Tolar (entire testing period), Armazones (since January 2007) and Tolonchar (since March 2007), but are not part of the standard site setup. The AWS sensors are installed between 1.5 and 2.5 m above the ground.

At each site, a sonic anemometer (CSAT-3 model by Campbell Scientific) is placed at the level of the MASS/DIMM telescope, 7 m above the ground. It measures a "sonic temperature" (proportional to temperature, but also dependent on humidity and other parameters) and wind speed and direction. The raw data for turbulence measurements are also taken and saved.

On recommendation by the External Advisory Panel, we installed 30 m towers on Armazones (September 2006) and Tolonchar (March 2007). These are equipped with sonic anemometers and air temperature sensors at the 11, 20 and 30 (or 28) m levels. A 30 m tower was also set up and operated by the LSST project at San Pedro Mártir from December 2005 to May 2006. It was equipped with Metek USA-1 sonic anemometers at the 7, 12, 19 and 30 m tower levels. The base of the San Pedro Mártir 30 m tower was approximately 6 m below the base of the MASS/DIMM telescope tower. This difference is $\sim$2 m at Tolonchar and less than 1 m at Armazones.

Data from the AWSs are downloaded once every two minutes, except when there is a 30 m tower installed at the site, in which case they are read once every minute. The stations are configured such that the delivered values are averages over the previous minute. The temperature probes on the tower are set up to produce measurements every 2 seconds. These measurements are instantaneous values. Sonic anemometer raw data are taken and saved at 60Hz. Currently, only averages of one-minute subsets of the sonic data are analyzed. If desired, the raw data can be used for temporal power spectra analyses at a later time.

Note that the vendor accuracies quoted in the following subsections are valid for one year. After that time, the sensors should be sent back to Monitor Sensors for recalibration. This is done on an as-needed basis for the TMT site testing equipment.

6.1.1 Temperature (AWS and Sonic Anemometers)

The measurements of the temperature sensors are routinely compared to hand-held thermometers during site visits. These comparisons have an accuracy of approximately 2°C and serve to identify gross malfunctions of the sensors.

In order to establish temperature differences and temperature gradient differences between the sensors on the 30 m tower that are useful as inputs for CFD simulations, a much higher accuracy and reproducibility ($\sim$0.1°C) are required. We have therefore undertaken several side-by-side comparisons of sonic anemometers and AWSs. It turns out that an absolute temperature

calibration to fractions of a degree Celsius is not trivial, but can be achieved if co-calibrated temperature sensors are used [*Skidmore07a, Riddle07a*]. It is also necessary to have the sensors re-calibrated by the vendor periodically.

The sonic temperatures measured by several sonic anemometers at the same site are well correlated with each other. There are, however, offsets between the individual instruments of up to 3°C that require an additional investigation [*Skidmore06a, Skidmore07a*]. As AWS temperature sensors are installed at all locations of interest to TMT, we are currently not pursuing this further.

6.1.2 Wind (AWS and Sonic Anemometers)

Wind speed and direction are compared to hand-held wind sensors and a compass during site visits. The accuracies of these comparisons are approximately 2 m/s and 5°, respectively, and are used to determine serious malfunctions of the sensors.

The vendor quoted accuracies of the AWS and sonic anemometer wind speed measurements are 2% and 0.04 m/s, respectively. As with the temperature measurements, confirmation of these accuracies is not simple, as difference between instruments at the same site are usually dominated by local effects, such as units being up- or downwind from each other or from other structures [*Skidmore07a, Riddle07a*]. Results from comparisons of the tower probes on both Armazones and Tolonchar show that the accuracy is better than 5%, which is most likely limited by the experimental setup rather than the probes themselves. It is therefore a conservative limit.

The wind direction measurements are limited mostly by the setup accuracy of the instruments and are estimated to be better than 5° [*Skidmore07a, Riddle07a*].

It should be noted that the AWS wind sensors contain moving parts and are therefore much more prone to failures than other AWS sensors. They can also freeze in cold and humid conditions. Our data sets are therefore periodically scanned for periods of zero wind speed or constant wind direction readings. We also analyze the statistical properties of the wind speed distributions and compare AWSs and/or sonic anemometers for the periods when more than one instrument was operating simultaneously at a site [*Skidmore06a, Skidmore07ab*]. It is possible to exclude suspect periods from the data analysis, if they can be identified unambiguously. The latter is, however, not always possible because of the more subtle effect of dust getting into the gears, which affects both the wind speed reading and the lowest measurement threshold. Excluding zero readings that are caused by low wind speeds and dust in the gears would bias the overall statistics just as much as not excluding zero readings in normal to high winds because of a completely stuck sensor. When in doubt, we therefore usually do not exclude data but add a warning in the corresponding result report instead. Tests show that biases of the overall statistics (for example, median values) are usually small.

Also note that the sonic anemometers at the MASS/DIMM telescope level are installed close to the telescope enclosures, which affect the wind flow. This effect is weaker during the night when the domes fold away entirely, but is still visible in the comparison of wind direction measurements between sonics and AWSs [*Skidmore07b*].

6.1.3 Humidity, Pressure, Solar Irradiance, Precipitation, Heat Flux (AWS)

The vendor quoted accuracies of the other AWS sensors are as follows: Humidity 2%, pressure 1 hPa at 25°C, solar irradiation 5%, heat flux 5%, and net radiation 3%.

Humidity and pressure readings are compared to hand-held equipment during site visits. The accuracies of these comparisons are on the order of a few percent and a few hPa. These accuracies are sufficient for TMT site selection purposes. A comparison between units on Armazones

[*Skidmore07a*], however, shows that humidity sensors can show significantly higher errors as well as "zones of avoidance", humidity ranges that they do not seem to measures. This is due to a non-linearity of this kind of sensor in the range around 30% humidity. Nevertheless, the accuracies achieved are still sufficient for TMT site selection purposes.

Solar irradiation measurements are not used in the site selection analysis and are therefore not verified independently. Furthermore, since the readings are affected by dust accumulation on the sensor, an absolute calibration would only be valid for a short period of time. A relative analysis of the data, for example to determine the presence of clouds during daytime, is possible, should this be desired at a later time.

We have no independent method of verifying the heat flux measurements. As these values are only needed for the SODAR calibration and only a crude estimate of the heat fluxes is required for that, there is no need to undertake such a calibration. The vendor quoted accuracy is significantly better than the required accuracy.

The precipitation sensors are only used to ensure the safety of the site testing equipment. No calibration is therefore undertaken.

6.1.4 Turbulence (Sonic Anemometers)

Sonic anemometers indirectly measure the turbulence strength, C_n^2, by measuring the speed of sound and therefore the local temperature fluctuations. Quantitative C_n^2 measurements are difficult because of the, at best, marginal temperature resolution and sampling frequency of the units [see *Oncley04* and *Socas-Novarro05*]. The determination of the optimum method to calculate C_n^2 from the sonic anemometer data and its accuracy is work in progress. Promising correlations with measurements from other instruments (microthermal sensors, SODAR and MASS) have been demonstrated, but we have not gone beyond the point of achieving qualitative measurements of the turbulence strength. For a description of this effort see *Skidmore06b*.

6.2 Differential Image Motion Monitors (DIMM)

Differential image motion monitors (DIMMs) are currently the standard for measuring the atmospheric seeing [*Sarazin90*]. A detailed description of the TMT DIMM systems is given in Section 9.5 of the SiRD and is not repeated here. The instruments were constructed at CTIO and are mounted on custom-made 35 cm telescopes manufactured by Teleskoptechnik Halfmann. At the candidate sites, the telescopes are installed on 6.5 m towers.[2]

6.2.1 Seeing

DIMMs derive the seeing[3] from differential image motion measurements and are therefore, to a limit, not affected by telescope vibrations. Furthermore, the only free parameters in the measurement are the plate scale of the detector and the subaperture diameters and separation, all of which can easily be measured with high accuracy. DIMMs are therefore often considered to be "fool-proof" and to require essentially no maintenance. As the seeing is an important factor in the TMT site selection process, we have gone to great lengths to determine the accuracy of the measurement and have

[2]The Tolar setup originally used a 3 m tower which was replaced by a 6.5 m tower on December 9, 2004. In principle, the DIMM data before and after this date should be treated separately. However, as there appears to be no significant difference between the data before and after this event (see Section 7), this is currently not done.

[3]All turbulence results given in this report, as well as in all other TMT site selection documents, are always calculated for a wavelength of 0.5 μm and observation at zenith.

found that the above assumptions are only true if accuracies of approximately $0\farcs1$ are sufficient and even then only if the telescope focus does not drift (the latter was known beforehand).

In a multi-month side-by-side comparison of several DIMM systems, including two of the TMT units (now at Armazones and Tolonchar) and two Meade-telescope based DIMMs, as well as a later comparison involving another of the TMT units (at San Pedro Mártir) and a Meade-based DIMM, we found that the optical alignment of the telescope/instrument system is critical if accuracies better than $0\farcs1$ are desired. We determined that the agreement between TMT units can be ensured to be $\sim0\farcs02$ or better with good optical alignment. We also determined that the Strehl ratio of the DIMM stellar images is a reliable metric of the alignment quality. This is described in detail in *Wang07*.

Determining the absolute error of the DIMM measurement is not simple. However, our calibration campaigns involved not only identical TMT DIMMs, but also Meade-based "Tololo-style" DIMMs (CTIO-DIMMs) which use a somewhat different method (two-dimensional vs. one-dimensional image motion measurements) as well as different hardware and independently developed software. Due to technical problems with the CTIO-DIMMs, a comparison to the same level as for the TMT DIMMs was not possible, but we could show that the results from the two systems differed by at most $0\farcs05$. Thus, we verified that the DIMM method has been implemented correctly in the TMT DIMMs. The DIMM method in general has been verified many times in the two decades since its invention. It is therefore likely that the absolute accuracy of our measurements is also better than $0\farcs05$ and that that is a conservative limit.

Having said that, several things should be noted.

- The given accuracies apply to the seeing statistics, not to the individual measurements, which showed an rms scatter of approximately $0\farcs1$ during the calibration campaigns. This can be considered an upper limit of the rms error of the individual measurements, as we have also shown that at least a part of this scatter was caused by real differences in local turbulence [*Wang07*].

- The quoted accuracy does not apply in high wind speeds. While the DIMM method is generally considered independent of vibrations, this is only true if the telescope motion is slow compared to the DIMM exposure time (6 ms for our units). If the DIMM exposures are smeared out by telescope vibrations, this is effectively the same as a bad optical quality of the instrument, resulting in the measured seeing value being worse than the actual seeing. Thus, DIMM measurements need to be taken with some care in high wind speeds. It should, however, be noted that, due to their robust hardware, our DIMM systems produce reliable measurements in much higher wind speeds than those of most or all other existing DIMMs. An investigation of the effect of vibrations [*Schöck07a*] shows that they are negligible for wind speeds up to $\sim$12 m/s. This is close to the operation limit for both our DIMMs (13.9 m/s) and for TMT (15.6 m/s). Even past this speed, the effect is small and can be neglected in the overall seeing statistics.

- Also note that the DIMM measures differential image motion. The seeing (image width) is computed from this measurement with the assumption of Kolmogorov turbulence. The relation between the two measures of turbulence has been extensively confirmed, both theoretically and empirically. It is, however, not the same as the image width a large telescope would see under the same conditions, as a finite outer scale of turbulence reduces the latter.

6.2.2 Isoplanatic Angle

The isoplanatic angle can be derived from the scintillation index of the DIMM data. In practice, this measurement is difficult with the TMT DIMMs as the frame exposure time fluctuates slightly in time. This introduces an additional apparent scintillation term to the data, which can be significant for weak high-altitude turbulence (large isoplanatic angles). Routine DIMM measurements of the isoplanatic angle are, however, not required as reliable measurements are obtained with the MASS (see Section 6.3.2). Thus, the DIMM isoplanatic angle measurements are only used to verify the general validity of the MASS measurements.

6.2.3 Turbulence Coherence Time

A method to calculate the turbulence coherence time, τ_0, from a continuous series of DIMM data was investigated in *Lopez93*. The accuracy of the results were found to be uncertain as they depend on the turbulence and wind (both speed and direction) profiles, which are generally not known. Thus, a determination of the turbulence coherence time from the TMT DIMM data will likely not be possible with high accuracy. DIMM data are therefore only used to verify the general validity of MASS τ_0 measurements, which have the advantage of not depending on the wind direction (see Section 6.3.3).

6.2.4 Cloud Cover and Transparency

The determination of cloud cover and transparency using DIMM data is analogous to that using MASS data (see Sections 6.3.5 and 6.3.6). Since the MASS uses a single photo multiplier per subaperture rather than a CCD, it is more conveniently suited for this analysis. A full analysis of cloud cover and transparency using DIMM data is therefore unnecessary and is only performed for selected periods in order to validate the MASS-based method.

6.3 Multi-Aperture Scintillation Sensors (MASS)

Integrated in the same physical instrument as the DIMM is a Multi-Aperture Scintillation Sensor (MASS). The MASS/DIMM units were built in a collaboration between CTIO and the Sternberg Astronomical Institute in Moscow, Russia. A MASS produces six-layer measurements of the turbulence profile, excluding the first few hundreds of meters [*Kornilov03*]. The layers are centered around 0.5, 1, 2, 4, 8 and 16 km elevation. The ground layer turbulence strength can be calculated from the difference between the DIMM and MASS seeing.

Although the MASS instrument is quickly becoming the standard for turbulence-profiling using small (tens of centimeter diameter) telescopes, neither the reproducibility nor the accuracy of the measurements were known at the beginning of the TMT site selection campaign. We therefore have undertaken a large effort to understand the calibration and uncertainties of the TMT MASS instruments. The results of this effort, as well as of investigations by the MASS team, are summarized below and are described in detail in several supplementary documents [*Els06ab, Els07cde, Els08cd, Tokovinin06ab*].

6.3.1 Seeing and Turbulence Profiles

The MASS measurements described above are produced directly after data acquisition by the real-time software `turbina`. Originally, the MASS system worked only with `turbina`, not permitting a later reanalysis of the data. The MASS developers have since provided the reprocessing package `atmos` [*Kornilov05*] with which the previously acquired data can be reanalyzed. This package

is improved in its turbulence reconstruction schemes and allows the turbulence profiles to be recomputed with the proper instrument settings, which can in part only be determined after the measurements were taken. All data presented here and in the Results Update Report have been derived by reprocessing the raw MASS data using the `atmos` package.

The output of the original real-time MASS data analysis software `turbina` is based on the weak turbulence assumption and is known to have problems in the medium or strong scintillation regime. These problems manifest themselves by over-estimating the total seeing (referred to as MASS "overshoots") and locating turbulence lower than where it occurs. These issues have been investigated and solved by the MASS developers using simulations [see *Tokovinin06a*] and are corrected during the data reprocessing.

In addition, an analysis of the sensitivity of the MASS results to the input parameters was performed using the reanalysis software. It showed that the MASS results are repeatable to better than $0\farcs01$ for the seeing and much better than $0\farcs1$ ($C_n^2 \mathrm{d}h \approx 2 \cdot 10^{-14}$ m$^{1/3}$) for the individual layers, if all critical input parameters to the analysis software are measured routinely for each MASS unit [see *Els06ab* and *Els08cd*].

This is consistent with results from a side-by-side comparison of several MASS units which was undertaken simultaneously with the DIMM comparison described above. The results show that the MASS units agree to better than $0\farcs05$ for the overall seeing. The agreement of the individual layer strengths is found to be $<0\farcs1$ for all layers and is significantly better than that for higher layers [*Els07c* and *Els08cd*]. The experimental seeing repeatability is thus shown to be consistent with that from the sensitivity analysis.

During some occasions, small-scale vignetting of some of the MASS units was present. As the MASS concept relies on the knowledge of the geometry of the entrance apertures, this triggered an investigation to what extent such vignetting affects the MASS results [*Els07c* and *Els08cd*]. It was found that the amount of vignetting found on occasion in the TMT MASSs is smaller than the inherent precision of the units. It therefore does not present a problem.

Assessing the absolute errors of the MASS data is more difficult. A comparison of SODAR and MASS results shows that the agreement is on the order of 10% for the lowest layers [see *Travouillon07*]. There are many other indications that the measured values are indeed close to the real seeing and turbulence profile, such as:

- MASS seeing values, after correction for over-shoots, are generally well bound by the DIMM seeing values.

- Investigations of anisoplanatism at both the Keck and Palomar AO systems show good agreement between measured point spread functions and those reconstructed from the MASS profiles [see *Britton06* and *vanDam06*].

- Other groups have also compared MASS units with other turbulence profilers such as SLODARs and SCIDARs, finding general agreement albeit of varying magnitudes.

- The ground layer seeing as computed from the difference of DIMM and MASS seeing can successfully be correlated with other atmospheric parameters measured by the meteorological stations [*Els07d*].

Thus, there is significant evidence that MASS units produce absolute measurements of the turbulence profiles with accuracies similar to the repeatability values given above.

6.3.2 Isoplanatic Angle

If the turbulence profiles have been measured correctly, the isoplanatic angle is also known. The side by side comparison of two MASS devices resulted in an agreement of the isoplanatic angle of better than $0\farcs02$ [*Els07ce* and *Els08cd*].

On an absolute scale, the accuracy of the measurements is not exactly known, but a general agreement with the DIMM isoplanatic angle measurements and the results of the PSF analyses [see *Britton06* and *vanDam06*] shows that the values are, at least, good approximations of the real isoplanatic angles. Based on a comparison of two different methods of calculating the isoplanatic angle, we estimate that the accuracy is better than $0\farcs2$, and likely much better than that [*Els07ce* and *Els08cd*].

6.3.3 Coherence Time

The MASS produces turbulence coherence time, τ_0, values as one of its standard outputs. The repeatability of these values was found to be approximately 0.1 ms in a side by side comparison of two MASS devices [*Els07e* and *Els08cd*].

A report investigating the accuracy of the MASS τ_0 values by the MASS team shows good correlations with other methods, but with significant, albeit relatively constant biases [*Tokovinin06b*]. It concludes that the intrinsic accuracy of the τ_0 estimate after correction and inclusion of DIMM data is expected to be 20% or better. These results were confirmed by us for all TMT candidate sites by a comparison of MASS τ_0 data with wind profiles from the nearest radiosonde balloon launch site. We confirmed that a correction factor to MASS τ_0 values is required. This factor appears to be the same from site to site to within $\sim$10%. We also determined that the ground layer seeing, as calculated from the DIMM - MASS seeing difference, contributes significantly to the overall τ_0. The resulting error of the τ_0 measurement is estimated to be 20%. See *Travouillon08a* for details.

6.3.4 Temporal Variability

The temporal variability of turbulence parameters such as MASS and DIMM seeing, isoplanatic angle and coherence time were also investigated. There are many different possibilities to define temporal variability metrics which have different practical meanings and also show different relative behavior of the sites. The methods and results are not shown here, they are reported in *Travouillon08bc*.

6.3.5 Cloud Cover

As both DIMM and MASS measure turbulence properties by observing bright stars, the received fluxes can, in principle, be used to assess cloud cover along the line of sight. In practice, this is complicated by the lack of knowledge whether the absence of star light is caused by clouds or technical or pointing problems. As cloud cover estimates are already obtained from all-sky camera (ASCA) data (see Section 6.6.1), a full cloud cover assessment from MASS data is not needed. Instead, we only use MASS data for the verification of the ASCA results.

6.3.6 Transparency

A MASS measures the flux coming from a bright star with four photo multipliers (one for each of the four MASS subapertures) at a frequency of 1000 Hz. Short-term variations of the flux can therefore be detected with high accuracy. In principle, one could also use the total flux received by the MASS

as a measure of extinction. In practice, this is complicated by effects such as the accumulation of dust on the optics and differences in sky brightness caused by the Moon. Instead, the LOSSAM (Line Of Sight Sky Absorption Monitor) method is used. This method was developed for the VLT Astronomical Site Monitor at Cerro Paranal.[4] It is based on the observation that the root-mean-square (rms) fluctuations of the flux from a bright star, averaged over several minutes and divided by the mean flux, are well correlated with the atmospheric extinction coefficient. As one-second rms and mean fluxes of the MASS measurements are saved to disk and archived for all our sites, the atmospheric extinction can thus be calculated in post-processing for all times for which MASS data are available. The method has been implemented and compared with sample data from the all-sky cameras (see also Section 6.6.1) and has been been shown to produce qualitatively correct results. A quantitative calibration was not undertaken [see *Schöck08b*].

6.4 Acoustic Sounders (SODAR)

SODAR (SOund Detection And Ranging) is the acoustic equivalent of RADAR. SODAR instruments have the capability of measuring both turbulence and wind velocity profiles in the atmospheric ground layer (GL) with high resolution. In order to study the lower part of the atmosphere, below the range of the MASS, we use a pair of SODARs that complement each other to sample elevations from 10 – 800 m. The first SODAR is a low range, high resolution model (SFAS by Scintec). We operate it in a way that it produces a turbulence and wind velocity profile from 10 – 200 m every 30 minutes, with a resolution of 5 m. The second model is a high power, high range SODAR (XFAS) that operates from 40 – 800 m with a vertical resolution of 20 m. The combined range of the two SODARs fills the elevation gap between the DIMM (7 m above the ground) and the first turbulence layer sensed by the MASS. TMT operates three sets which are rotated among the sites.

SODARs are notorious for their difficult calibration. In order to obtain quantitative results that are useful for TMT site selection, three steps were taken [see *Travouillon07*]:

- Turbulence Calibration: SODARs measure turbulence induced by the reflection of acoustic waves by temperature inhomogeneities. Unfortunately, acoustic absorption by air molecules varies with temperature, humidity and wind speed which makes it difficult to calibrate SODARs to give accurate values of C_n^2. We therefore went through significant efforts to devise and test a calibration method that uses our measurements of weather parameters available from the meteorological stations to compensate for the variations of the acoustic absorption. The base calibration is done near noon when the GL is fully convective. We can then use a broadly accepted and experimentally verified model of the convective atmosphere to calibrate our SODAR turbulence measurement.

  The complete details of the calibration and its procedure can be found in *Travouillon07*. As the calibration is instrument and site dependent, each SODAR was calibrated individually at each site. The accuracy of the calibration can be assessed from a comparison with MASS-DIMM results which is described below.

- SODAR cross comparison: In order to assess the reproducibility of our SODAR results across all sites, we have taken simultaneous SODAR measurement, both with two SODARs of the same model (SFAS/SFAS and XFAS/XFAS) and with different models (SFAS/XFAS). This cross comparison was done for both turbulence and wind speed profiles. It resulted not only in the quantification of relative errors of the instruments, but also identified a bias of the

[4] http://www.eso.org/gen-fac/pubs/astclim/lasilla/asm/lossam/

wind speed measurements. As large wind speeds mean large (acoustic) background noise, they result in a reduction of the signal-to-noise ratio (S/N) of the SODARs. When the S/N drops below a certain level, the SODAR cannot measure the wind speed, hence biasing the statistics of our wind speed profiles toward lower values. It is possible to correct at least approximately for this bias. The relative agreement between identical SODARs was then found to be better than 20% for the wind speed measurements. A wind speed offset on the order of 1 m/s between the two SODAR models was, however, observed. It remains unclear at this time if only one or both of the SODAR models contribute to this offset. The relative error of the seeing measurements was found to be ∼10%.

- Comparison with MASS-DIMM: The accuracies of our calibration and of the SODAR measurement of the integrated GL seeing were assessed by a comparison with the GL seeing measured from the MASS-DIMM difference. It shows that the SODAR GL seeing correlates well with the MASS-DIMM (with the exception of San Pedro Mártir where the tree-induced acoustic noise is a problem; see below). It also led to the identification of and correction for a noise issue with the SODAR. We believe that this noise is a combination of ambient acoustic noise and internal electrical noise. This inter-instrument comparison was done at all sites in order to quantify the accuracy of our results for each set of SODARs at each site. The result is that the accuracy of the SODAR GL strength measurement is likely similar to its repeatability, that is, ∼10%.

As already noted, SODARs are very sensitive to acoustic noise in their environment. This includes echoes off structures, noise from buildings (air conditioning units etc.) and noise caused by the wind moving around structures or through trees. Thus, the reliability of results is reduced at sites containing such structures close to the SODARs. This applies in particular to San Pedro Mártir, but the wind noise produced by the site testing towers themselves, in particular the 30 m towers, is also an issue.

6.5 Dust Sensors

The dust sensors are commercial units from Met One Instruments. They measure the particle count in five different channels, for particle sizes 0.3, 0.5, 1.0, 2.0 and 5.0 μm. Here, the given size is a lower limit, each channel counts all particles with sizes equal to or larger than the respective value. The vendor quotes an accuracy of 10% for the individual measurement. We undertook a side-by-side calibration of the sensors in the lab in Pasadena to determine if the sensors performed to this specification, and to evaluate if sensors at various sites can be compared directly.

The calibration results are described in a separate document provided with this report [*Riddle06*]. We found that the differences between the sensors are generally below the 10% level quoted by the vendor. Only for the 2.0 and 5.0 μm channels did we find larger differences for some units. This is likely caused by the very small particle counts we encountered for these channels in the lab rather than by the inherent accuracy of the instruments. We also found that the differences tended to be systematic for the period of testing (7–10 days). After the end of the site testing campaign, we might undertake another cross-comparison of the dust sensors. If the same systematic differences are found then, a relative scaling of the values can be performed to improve the reproducibility of the measurements.

We have no means for an independent verification of the absolute errors (accuracy) of the measurements. This is, however, not needed, as a comparative particle count between the sites is sufficient for TMT site selection purposes. We therefore use 10% as estimate for the reproducibility of the dust sensor measurements and will not investigate their accuracy further.

6.6 All-Sky Cameras (ASCA)

All-sky cameras (ASCAs) have been deployed at all candidate sites. The TMT ASCAs are replicas of the Tololo ASCA and were built by CTIO.[5] A detailed description of the cameras is given in *Walker06*.

6.6.1 Cloud Cover and Transparency

Obtaining quantitative cloud cover and transparency measurements from all-sky images is a complex task. An automated photometry software package, originally written for the Canada France Hawaii Telescope (CFHT), has been adapted for us by Eugene Magnier of the Institute for Astronomy. The photometry analysis using this software package works well, but it turned out that the determination of cloud cover from the data cannot be done with an accuracy better than ∼10%. This is due to instrumental limitation (pixel size, signal-to noise ratio, etc.) and the method itself (for example, it is not possible to determine whether stars are not found due to clouds or due to other factors without employing pattern recognition software or a similar approach).

We therefore conducted a visual analysis of movies of all ASCA images [*Skidmore08a*]. The movies, each covering an hour of night-time data, were assigned one of the following categories:

1. No clouds are detected inside the 65° zenith angle TMT observing limit
2. Clouds are detected inside the 65° limit, but not inside a circle covering half the area on the sky (44.7° zenith angle)
3. Clouds are detected inside the 44.7° circle
4. Opaque clouds cover more than 50% (integrated over space and time) of the area inside the 65° circle
5. Periods with the moon up (meaning shorter exposure times), snow or condensation on the camera or other problems that make cloud detection difficult or impossible were given separate categories that were excluded from the statistical analysis.

These categories are not identical to what a TMT observer would consider "photometric", "spectroscopic" or "unusable" conditions. They were defined in this way because we found other categorization schemes to be too subjective to produce repeatable results. They are, however, consistent between sites and can be used for a comparison of the candidate sites for site selection purposes.

Out of the 118 months of ASCA movies from the five sites that were analyzed, 20 were analyzed by at least two people independently. A comparison of these overlap periods shows that the repeatability is ∼1% for Tolar, Armazones, San Pedro Mártir and Mauna Kea 13N and ∼4% for Tolonchar. The larger error for Tolonchar appears to be due to a more complex (and more difficult to analyze) cloud pattern and because it appears more difficult to distinguish thin clouds from sky glow there. For details about the method, its limitations and results see *Skidmore08ab* and *Schöck08b*, which also show a comparison with MASS LOSSAM data (see Sections 6.3.5 and 6.3.6).

As the deployment period of the ASCAs is too short for us to be certain that it is representative, TMT also contracted several satellite cloud cover and precipitable water vapor studies with the group of André Erasmus. The results of these studies were compared with the ASCA cloud

[5]The ASCA deployed at San Pedro Mártir is owned by LSST. Its images are available to TMT through a data-sharing agreement involving all instruments either project has deployed at San Pedro Mártir.

cover data and found to be consistent [see Section 6.9]. We thus confirmed that the satellite data measure clouds in a consistent way. Cloud cover statistics for the TMT candidate sites are therefore determined from satellite and climate data, which cover up to 10 years of satellite data and up to 27 years of NCEP reanalysis data.

6.6.2 Usable time

ASCA cloud cover data can be combined with simultaneous measurements of other parameters that might prevent TMT from operating, such as high humidity and wind speed. We can then determine which fraction of time these conditions occur while it is clear and the additional loss of observing time they cause. The results are, however, dependent on the exact shutdown conditions used for TMT at the candidate sites, which are not yet known and which might be site dependent. Only ranges of additional observing time lost due to weather other than clouds can therefore be given (see *Schöck08b* for details).

6.6.3 Light Pollution and Sky Brightness

We also analyzed light pollution as a function of zenith distance using ASCA images. Nights around New Moon with no clouds present are selected for this purpose. All images of a night are median stacked and the darkest 10% values are determined for each pixel in order to eliminate stars. The results are then normalized with respect to the zenith conditions. By looking at this normalized sky brightness as a function of zenith angle in 15-degree azimuthal slices, we can then determine in which direction artificial light sources are detectable. We found that all sites are very dark, but that each sites has a number of directions in which light pollution is detectable close to the horizon. The vertical extent of the light pollution visible in the ASCA images is very close to the horizon under most conditions, and barely reaches the 65° observing limit of TMT under the worst conditions (usually meaning low clouds on the horizon). For a description of the method and the results see *Riddle08* and *Schöck08c*. The directions in which light sources are visible at each site are described in Section 4.

A quantitative analysis of sky brightness is not possible from the ASCA images because the cameras are not calibrated in an absolute sense, or even relative to each other, and due to instrumental limitations such as the pixel size, the sensitivity of the instruments and the signal-to-noise ratio of the images.

6.7 Infrared Water Vapor Radiometers (IRMA)

Three Infrared Radiometer for Millimetre Astronomy (IRMA) units were contracted to the University of Lethbridge. An IRMA measures the sky flux around 20 μm ($\sim$16.5 – 21.5 μm) wavelength and derives a precipitable water vapor (PWV) value from this flux by use of a suitable atmospheric model. The devices were first delivered at the end of January 2006 and tested side-by-side during three weeks on Cerro Paranal. Unfortunately, problems with the hardware and calibration method were discovered which required significant work on the units. This was completed at the end of 2006.

The three units were redeployed for another round of side-by-side comparisons on Armazones in January of 2007. The results show that there is a good correlation (repeatability) between the units that is stable on the $\sim$0.25 mm level over the range of PWV values encountered during the tests ($\sim$2 – 20 mm). However, offsets between the units on the order of 0.5 mm exist in the side-by-side comparison. In a comparison with data from other instruments (see Section 6.10), we have further shown that the IRMA data correlate well with other data sets, but that offsets with respect to

the other data can be as large as several millimeters of PWV and that they are site dependent (atmospheric model dependent). Thus, IRMA data are only used to analyze the shape of the PWV distributions [see *Schöck08a*]. Representative PWV data for the sites are found from satellite data, other radiometers installed at Mauna Kea and San Pedro Mártir and radiosonde balloon data (see Sections 6.9 and 6.10).

After the comparison campaign on Armazones, one IRMA unit remained there, one was moved to Mauna Kea 13N in February 2007, and the third was moved to Tolonchar in March 2007.

6.8 Computational Fluid Dynamics

Many computational fluid dynamics (CFD) simulations have been performed for the TMT candidate sites. Besides simulations of the site conditions themselves, these include comparisons with radiosondes and site testing equipment on Tololo, analyses of the sensitivity of the simulation results to the input parameters for San Pedro Mártir, Mauna Kea and Tolonchar, and a study comparing changes in conditions predicted by CFD with on-site measurements [see the references in Section 8]. These studies show good qualitative agreement between measurements and simulations. Quantifying the agreement will be done during the site characterization phase (after down-selection to two sites), when we are planning to have several site testing stations deployed at the same site in order to monitor the turbulent flow over the site.

CFD simulations are also used extensively in the analysis of other aspects of TMT, such as dome and mirror seeing and wind buffeting. These efforts are reported elsewhere and are not presented in this report.

6.9 Satellite Data Analysis

Several Satellite studies of cloud cover and precipitable water vapor (PWV) at the TMT candidate sites were done by Dr. D. André Erasmus and his group [see the references in Section 8]. The results of the earlier studies were used for the pre-selection of candidate sites, as described in Section 4 of this report and in Section 8 of the SiRD. The main purpose of the later studies was to provide result that are simultaneous with the data taken at the sites. A comparison of satellite and ground data then provides a verification of the satellite results and upper limits to the error bars on both. The ground based data can then be put into the context of a study of 28 years of climate parameters from the National Centers for Environmental Prediction (NCEP) reanalysis data set (also done as part of the final study of the Erasmus group; see *Ivanescu07ab*) in order to judge whether the conditions encountered during the site testing period were representative for the long-term conditions at the sites.

The comparison of simultaneous satellite and ASCA cloud cover data (see Section 6.6) shows that the two data sets are consistent with each other to within <2% for Tolar, Armazones, San Pedro Mártir and Mauna Kea 13N. 'Consistent' here does not mean equal numerical values, as the two data sets do not characterize exactly the same cloud properties, but that the relative behavior of the sites is the same. Tolonchar deviates from this behavior on the 6% level. This is due to the larger errors in both the satellite and ASCA results (both of which are likely caused by the topography around Tolonchar which is more complex than that around the other sites) and are therefore an upper limit on the errors of the satellite cloud cover results.

In summary, we have shown that the satellite studies analyze cloud cover accurately within the errors given above. The satellite data are therefore used as our best estimates of cloud cover at the candidate sites for TMT site selection purposes, with the caveat that the Tolonchar results might be less reliable than those of the other sites. See *Skidmore08b* and *Schöck08b* for details and results.

A similar comparison of simultaneous satellite and ground PWV data was attempted but abandoned because the results of the satellite study covering the period simultaneous with ground data turned out to be unreliable. By contrast, PWV results from the previous satellite data studies appear to describe the conditions at the sites accurately, with an error estimate of 10–20%. As we do not have reliable ground-based data sets for all candidate sites (see Sections 6.6 and 6.10), the results from the 2003 Erasmus study comparing sites in Hawaii, the south-western USA and northern Chile [*Erasmus03*] are therefore used as the baseline for comparing PWV conditions at the TMT candidate sites. See *Otárola08* and *Schöck08a* for details and results.

The climate studies of meteorological conditions affecting cloud cover and PWV at the TMT candidate sites show that there appears to be no significant trend over the last 28 years [see *Ivanescu07b].*

6.10 Data from Other Sources

San Pedro Mártir and Mauna Kea are sites of existing observatories which, over the years, have seen many site characterization efforts. Data on image quality and environmental conditions from the observatories themselves are also available. In addition, the closeness of Armazones to Paranal might make some of the large amount of data from the VLT Astronomical Site Monitor applicable to Armazones.

It is, however, important to recognize that a reliable comparison of results is only possible if great care is taken to calibrate all instruments, operate them under controlled conditions and apply analysis criteria in equivalent ways. As was seen in previous parts of this section, it is difficult to achieve this even for identical instruments. The comparison of results for non-identical instruments that have not undergone the same kind of stringent calibration and data control procedures can easily lead to misinterpretations of the results. This is the main reason why the TMT site selection project put such importance on the use of identical equipment at all candidate sites and on rigorous characterization of our instrument suite. *Thus, a straight comparison of our results with those from other campaigns will, in most cases, not be meaningful and is generally not attempted as part of the TMT site selection process.* We made three exceptions from this.

First, it is, in principle, possible to get an indication whether the conditions encountered during the period of TMT on-site testing were representative if data sets from instruments that have been operating for longer times are available. This is analogous to the approach taken with the satellite data studies. Even then, such results have to be taken with care, as it is essential for this analysis that all input parameters and conditions (referring to both software and hardware) have been controlled and recorded consistently for the entire data acquisition period. As an example, in an attempt to verify whether the windier year of 2007 is more representative for Armazones than the less windy previous two years, we analyzed a 20-year time series of Paranal wind data. The results were inconclusive as construction of the VLT and VST produced changing conditions for the Paranal anemometers. It was not possible for us to disentangle the effects of the buildings and of relocating the wind sensors from changes in atmospheric conditions. Thus, in the end no such studies were used for TMT site selection purposes, other than the climate studies described in Section 6.9.

Second, we conducted several studies with the goal of verifying that our results are consistent with data from existing observatories and other site testing studies. These include the analysis of the sky transparency at Mauna Kea using CFHT SkyProbe data [*Steinbring06*], comparisons of Mauna Kea 13N seeing measurements with DIMM and image quality data from several observatories on the summit ridge [*Schöck06, Racine06ab, Chun06*], a comparison of different DIMMs at San Pedro Mártir [*Schöck07b*], an analysis of San Pedro Mártir 215 GHz radiometer data [*Otárola08*] and a

comparison of MASS and DIMM data taken simultaneously on Armazones and Paranal [*Schöck07c*]. We found that all of the other results are consistent with our data within the uncertainties of the comparisons, but that, for the most part, those uncertainties are too large for those data sets to be useful for TMT site selection purposes.

Third and most importantly, PWV data from other instruments were used in order to assess conditions at the candidate sites and to judge whether the satellite PWV results are reliable. This became necessary after the IRMA results turned out to contain large additive offsets that vary from site to site (see Section 6.7) and could not be used for this purpose. Thus, data from other radiometers operating at frequencies around 200 GHz at Mauna Kea 13N, San Pedro Mártir and at the ALMA plateau (for reference) and from radiosonde balloons launched in Hilo, Antofagasta and near San Diego were analyzed and compared with IRMA and satellite data. This provided the error bars for the IRMA data and verified that the 2003 satellite study (*Erasmus03*) provides accurate measures of the PWV conditions at the sites. By contrast, the final satellite study done for TMT (*Ivanescu07ab*) turns out to be not sufficiently reliable as far as PWV results are concerned (while the cloud cover results are reliable within the uncertainties given in Section 6.9). Details are given in *Otárola08* and *Schöck08a*.

6.11 Other Reports

An study of the air traffic in Chile's *II Región*, in which all of the TMT candidate sites are located, and its impact on TMT was also conducted and is attached as a supplementary document [*Els06c*].

7 TMT Site Selection Results

This section provides a top-level summary of the results from the TMT candidate sites. Detailed results are given in the TMT Site Selection Results Update Report [*Els08a*] and in the 30 m Tower Report [*Els08b*], which are provided together with this Site Selection Report. Some additional results are also given in the other references listed in Section 8. A description of the TMT site ranking metric and the results of its application to the candidate site data are given in the TMT Site Merit Function report [*Nelson08*].

7.1 Available Results

The Results Update and Tower Reports contain the following information.

Statistics covering the entire on-site testing period:

- DIMM, MASS and ground layer (GL) seeing and isoplanatic angle statistics
- MASS turbulence profile statistics
- SODAR seeing, wind and turbulence profile statistics
- Night- and daytime meteorological parameter statistics at the 2 and 7 m levels
- Night- and daytime wind roses for the 2 and 7 m levels
- Daily temperature / temperature gradient statistics for the 2 and 7 m levels
- Daily wind speed / wind speed gradient statistics for the 2 and 7 m levels
- Daily minimum, maximum and sunset temperature and wind speed statistics
- Correlations between DIMM, MASS, GL seeing and wind speeds at 2 and 7 m levels
- Dust sensor particle counts
- Ground and energy property statistics (soil temperature, energy fluxes)
- Temperature and wind speed profiles along the 30 m towers
- Temperature and wind speed gradient profiles along the 30 m towers
- Statistics of meteorological parameters for each level of the 30 m towers
- Daily temperature / temperature gradient statistics for each level of the 30 m towers
- Daily wind speed / wind speed gradient statistics for each level of the 30 m towers

Monthly statistics:

- DIMM, MASS and ground layer (GL) seeing and isoplanatic angle
- Meteorological parameter statistics at the 2 m and 7 m levels
- Meteorological parameter statistics for each level of the 30 m towers

These results are presented as plots and as tables containing cumulative histogram values.

Also given are comparative plots of the candidate sites for the following properties:

- Monthly DIMM and MASS seeing, isoplanatic angle, temperature and wind speed
- Cumulative DIMM and MASS seeing, isoplanatic angle, temperature and wind speed
- Median MASS turbulence profiles

Some results are also given in the other reports listed in the references, in particular:

- Precipitable water vapor [*Otárola08*, *Schoeck08a* and references therein]
- Cloud cover and usable time [*Skidmore08b*, *Schoeck08b* and references therein]
- Light pollution [*Riddle08*, *Schoeck08c*]
- Temporal variability of turbulence parameters [*Travouillon08bc*]
- Turbulence coherence time [*Travouillon08a*]

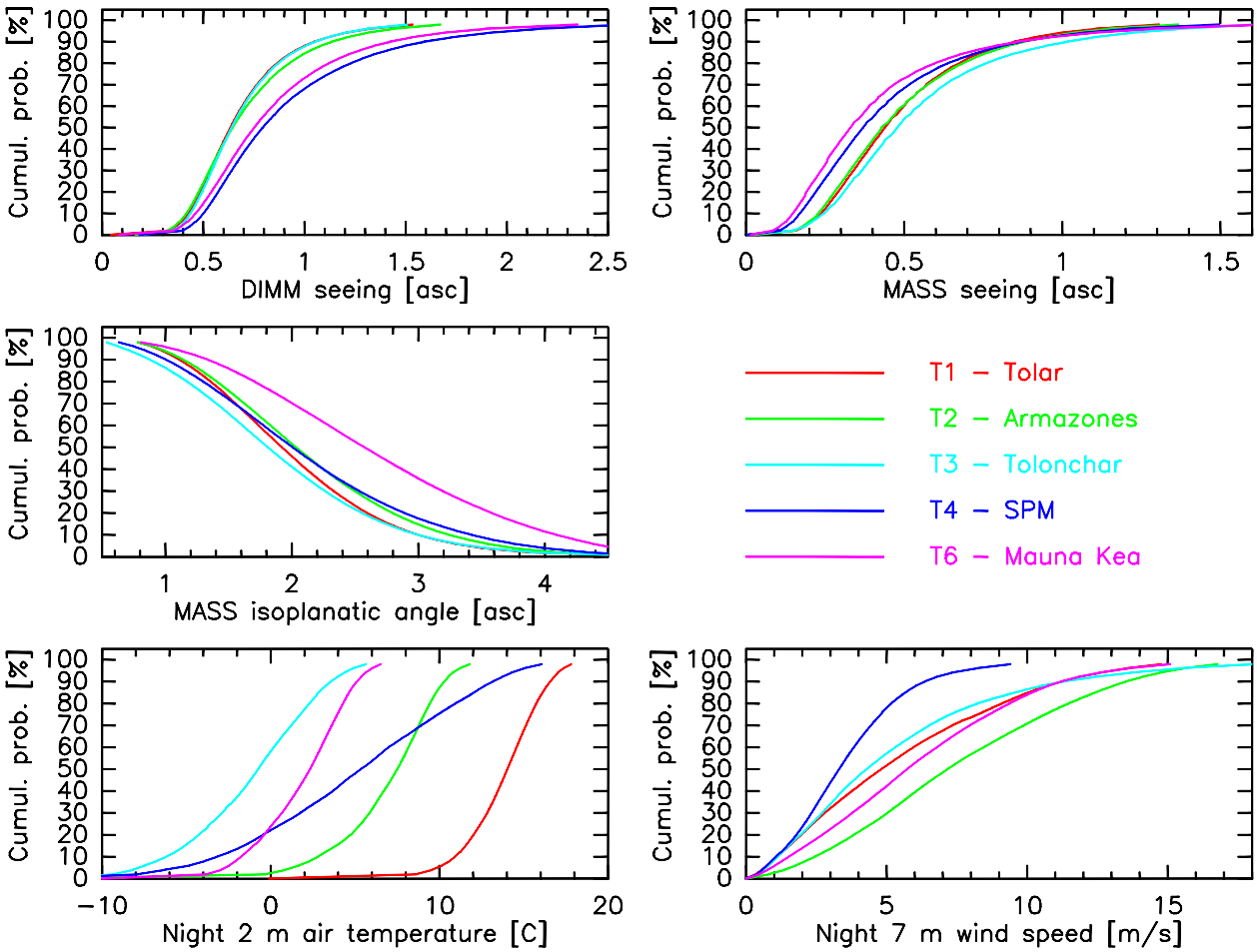

Figure 3: Cumulative probability distributions for the five candidate sites. DIMM and MASS seeing, isoplanatic angle, temperature and wind speed are shown.

The TMT site testing data are available in a database and can be downloaded using a web interface on the TMT site testing web site. This site also list known issues with the data sets, such as periods when sensors malfunctioned and data need to be excluded or if certain data require post processing. The web site is currently only accessible with a password. It will be made publicly available at some time in the future.

7.2 Summary of the Main Results from the Candidate Sites

Plots comparing the main characteristics of the TMT candidate sites are presented in Figs. 3 through 7. Figure 3 shows the cumulative probability distributions for each site for DIMM and MASS seeing, MASS isoplanatic angle, nighttime air temperature at 2 m above the ground and nighttime wind speed at 7 m. It can be seen that the total seeing, as measured by the DIMM, is smaller at the Chilean sites than at the North American sites, with Tolar, Armazones and Tolonchar being almost identical. San Pedro Mártir has a somewhat stronger total seeing at 7 m above the ground than Mauna Kea 13N.

For the MASS seeing (the seeing integrated from ∼500 m to the top of the atmosphere), the situation is reversed, with Mauna Kea 13N showing the weakest high-altitude turbulence, followed by San Pedro Mártir, Tolar/Armazones and Tolonchar. This shows that the larger DIMM seeing

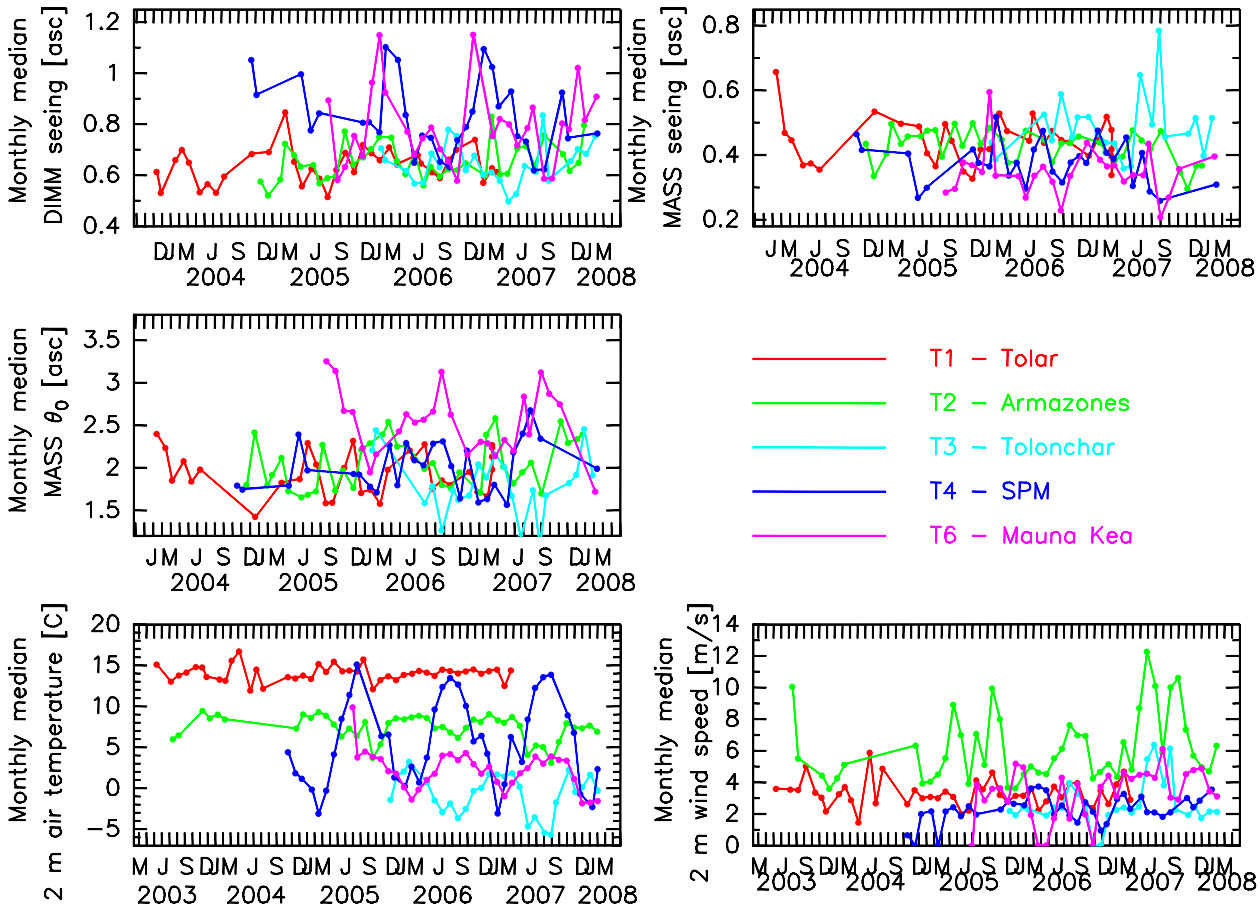

Figure 4: Monthly median values for the five candidate sites. The DIMM and MASS seeing, isoplanatic angle, temperature and wind speed are shown. Only months for which at least 1000 individual measurements are available (∼5 nights of data) are included in the plots. The AWS 2 m wind speeds are shown here instead of the 7 m sonic anemometer measurements because the AWSs have been operating at the sites for much longer than the sonics.

of the North American sites comes from their having a stronger ground layer than the Chilean sites (see also Fig. 5 and discussion thereof).

The isoplanatic angle behavior is similar to that of the MASS seeing, with the exception that San Pedro Mártir does not have an isoplanatic angle significantly better than the Chilean sites. The high-elevation turbulence profile at San Pedro Mártir, while having a lower integrated value than the Chilean sites, has a highest (16 km) layer which is approximately equally as strong as those of the Chilean sites (see Fig. 6). As the isoplanatic angle is dominated by high altitude turbulence, this causes the isoplanatic angle of San Pedro Mártir to be comparable to that of the Chilean sites.

The shapes of the temperature distributions in Fig. 3 are similar for Tolar, Armazones, Tolonchar and Mauna Kea 13N, with the slightly flatter shape of the Tolonchar curve indicating a little more seasonal variability than the other three sites (see also Fig. 4). The median values are a reflection of the site altitudes, Tolar being the lowest and warmest and Tolonchar being the highest and coldest. The median value of the San Pedro Mártir temperature also follows approximately this trend in altitude (it is somewhat colder than Armazones, which is of similar height), while the shape of the curve indicates a much larger annual temperature range. This stems from the fact that temperatures at San Pedro Mártir show much larger seasonal variations than at the other sites.

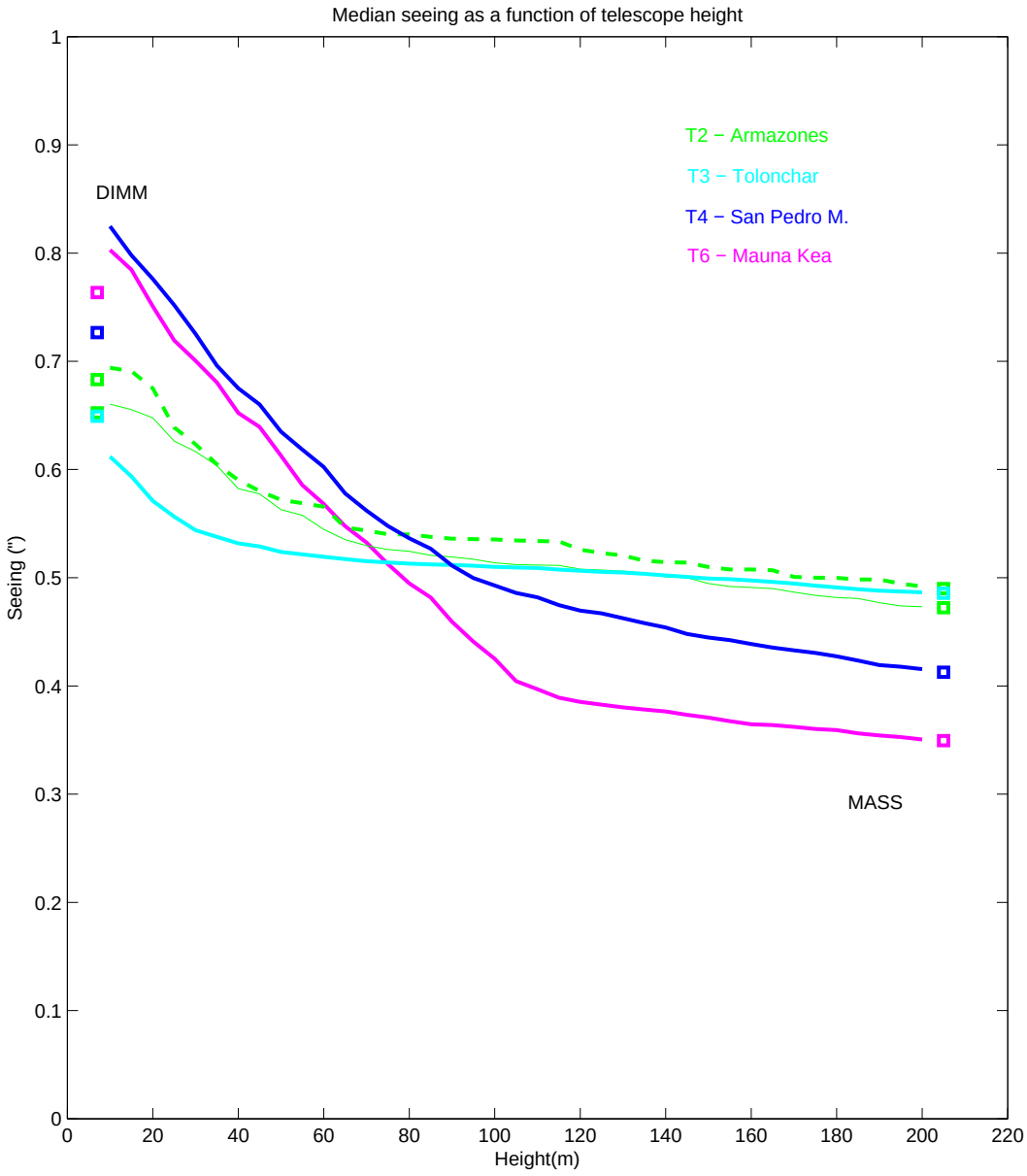

Figure 5: Median seeing an observer would experience at a given height above the ground as calculated from the MASS, SODAR and DIMM turbulence measurements (simultaneous data only). Note that the data cover much shorter periods of time than the overall site testing period, which means that these data should not be used to compare the absolute magnitudes of the ground layer seeing between the sites. They can, however, be used to get a general feeling for the shape of the ground layer profiles at the sites. See text for details.

Finally, the wind speed distributions (sonic anemometer wind speeds at 7 m) show Armazones

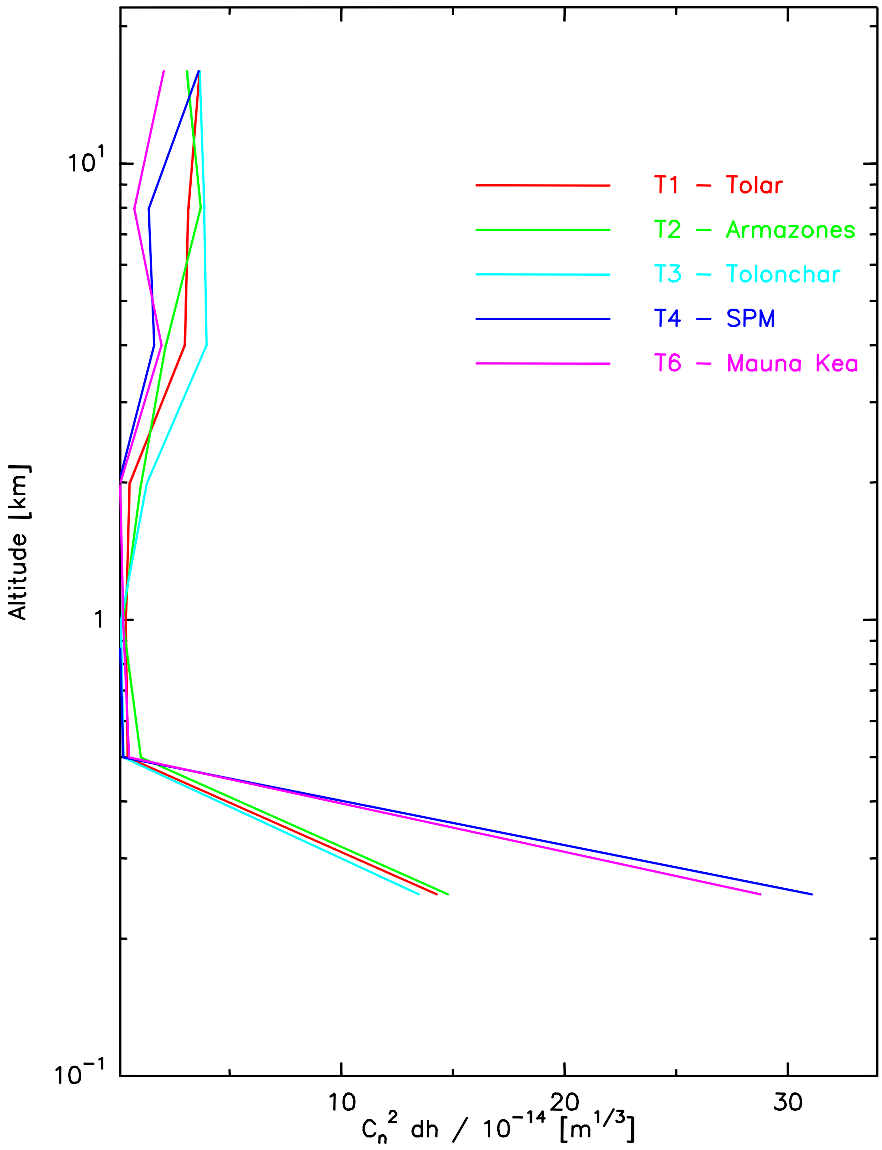

Figure 6: Median turbulence strength ($C_n^2 \mathrm{d}h$) profiles for the five candidate sites. The top six levels are the MASS profiles, while the lowest point (plotted here at 250 m) is the ground layer strength as calculated from the difference between the DIMM and the MASS seeing.

as the windiest site, followed by Mauna Kea 13N and Tolar. Tolonchar has surprisingly low wind speeds for a high-elevation site. Note that the free-air wind speeds at San Pedro Mártir are higher than indicated by our measurements which are affected by the presence of trees at the site. This effect is more significant for the 2 m AWS wind speed sensor than for the 7 m sonic anemometer, but it is not negligible for either instrument. Based on data from the 30 m tower at San Pedro Mártir [*Els08b*] and on existing data from the observatories, it appears that the nighttime wind speed measured by the sonic anemometer underestimates the free air flow by a factor 1.5 – 2.

Also note that, while the 7 m wind speed at Armazones is higher than at the other sites, its wind speed profile is essentially flat above that. This means that the wind speed differences between Armazones and the other sites at the level of the TMT enclosure openings are smaller than at the 2 m and 7 m levels.

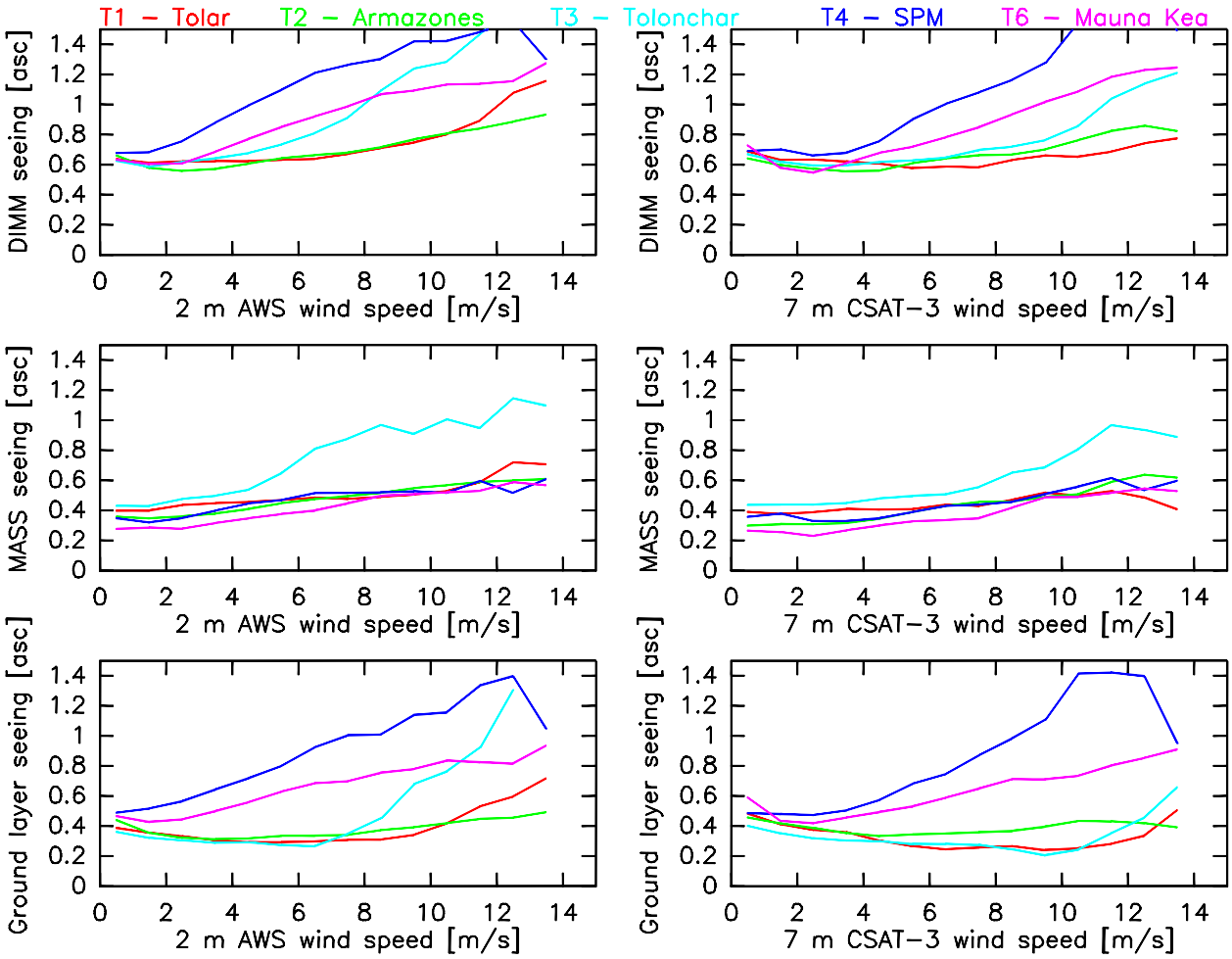

Figure 7: Median values of the seeing as a function of wind speed. DIMM (top), MASS (center) and ground layer (bottom) seeing are shown vs. the wind speeds as measured by the weather stations at 2 m (left) and the sonic anemometers at 7 m (right).

The variations of the monthly median values of the DIMM and MASS seeing, MASS isoplanatic angle, nighttime air temperature and nighttime wind speed at 2 m are given in Fig. 4. Note that the interpretation of outlying points in this figure requires the consideration of the number of data points available for each month. A point could be above or below average simply because it only contains a few days of measurements that are not representative of average conditions. This information cannot be given here without obscuring the plots. It is available in the plots for the individual sites in the Results Update Report. Also note that not all the ordinates of the graphs start at zero.

None of the turbulence-related properties of the Chilean sites display a strong seasonal variability, while the DIMM (and therefore the ground layer) seeing is significantly larger in the winter for the North American sites than in the summer. Also, the MASS seeing and, in particular, the isoplanatic angle appear to be seasonal at Mauna Kea 13N. There is little seasonal variation of average temperature for Tolar and Armazones, with some variation for Mauna Kea 13N and Tolonchar. San Pedro Mártir shows the strong seasonal temperature variation noted above. There is some evidence for small seasonal variations of the wind speeds for most of the sites, in particular also for Armazones. It should also be noted that the winter of 2007 was harsher (significantly more

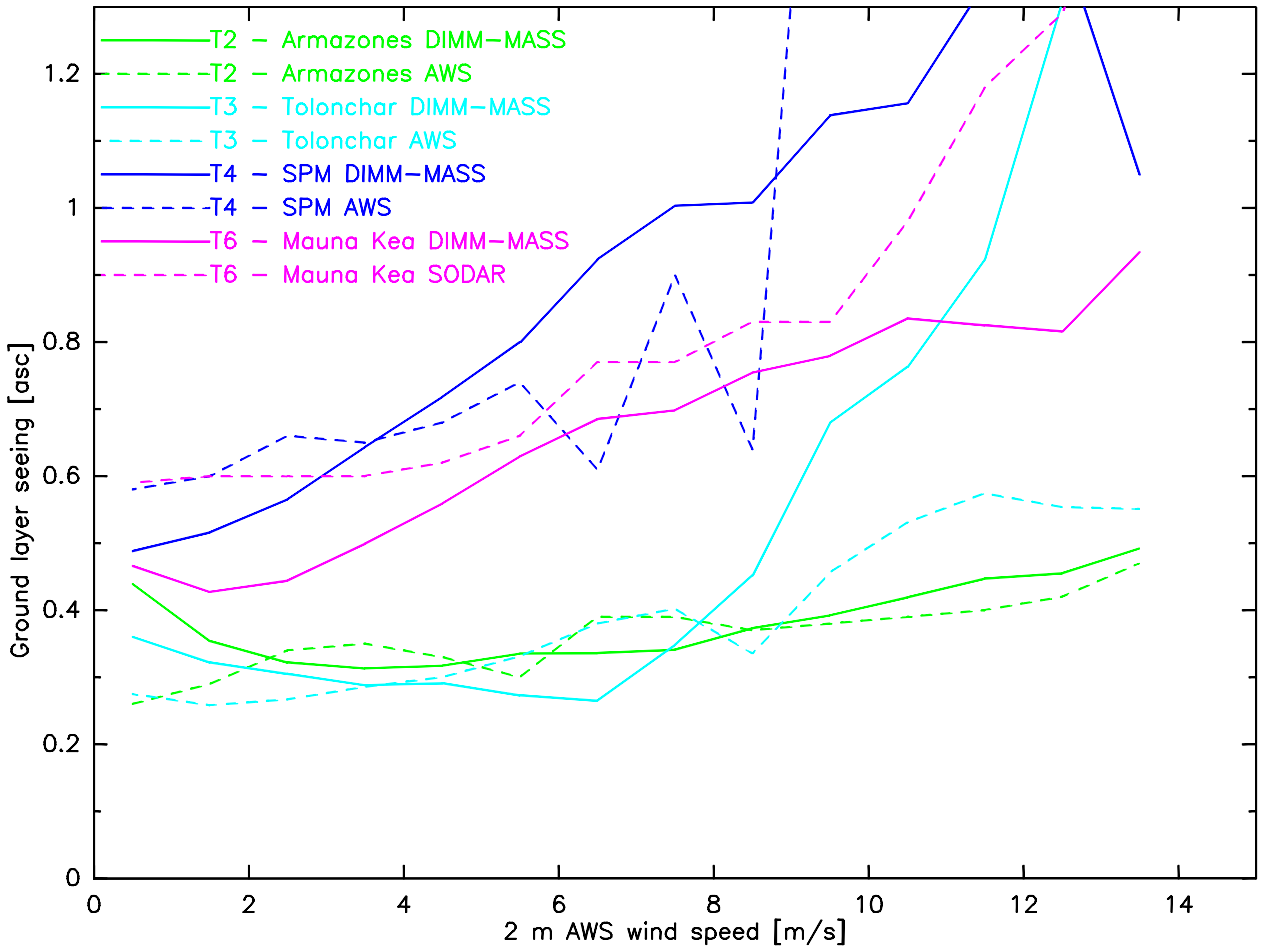

Figure 8: Median values of the ground layer (GL) seeing as a function of wind speed. The GL as calculated from the DIMM/MASS seeing difference (solid lines) and from the SODAR profiles (dashed lines) are both shown for the sites for which SODAR data exist. The AWS 2 m wind speeds are used here instead of the 7 m sonic anemometer measurements because no sonic anemometer data exist for the SODAR operation period on Armazones. As was the case for Fig. 5, the data shown here are not necessarily representative of average conditions at the sites. See text for details.

windy and somewhat colder) at the Chilean sites than the previous winters for which we have data. This is also reflected in the Tolonchar MASS data.

The results of the ground layer measurements from the SODAR are shown in Fig. 5. The quantity plotted here is the seeing encountered by an observer at a given height above the ground. The square on the right is the median MASS seeing (the seeing from approximately 500m up; plotted here at the 205 m level, for ease of presentation). The square on the left shows the median DIMM seeing, plotted at the DIMM elevation of 7 m. Only DIMM and MASS data that were taken simultaneously with the SODAR data are used for this plot. The curves are the sums of MASS seeing, XFAS SODAR seeing from 200 to 500 m and the SFAS SODAR seeing from the height given by the abscissa to 200 m. Individual profiles are added first and the median is calculated afterward. There are two curves given for Armazones as two SFASs were working there simultaneously. Note that there is no gap in elevation between the lowest elevation measured by the SFAS SODAR and the DIMM elevation. The lowest SFAS layer is designated the '10 m' layer, but is really an integral

from 7.5 – 12.5 m. Furthermore, the SODARs at all sites are set up ∼1 – 3 m below the base of the 6.5 m DIMM tower. Thus, no turbulence is missed by the SODAR that would be seen by the DIMM.

It must be noted that the SODAR data do not cover representative amounts of time for all seasons at all sites. Thus, the curves shown here should not be taken as representative for the long-term conditions at the sites. Nevertheless, several conclusions can be drawn. First, the good agreement between the DIMM seeing and the sum of SFAS, XFAS and MASS seeing is evidence that all instruments measure results that are comparable on the <10% level for all sites except San Pedro Mártir. (The discrepancy for SPM is caused by the noise created by the trees at the site which makes it difficult, at best, to calibrate the SODARs; see Section 6.4.) This supports the conclusion that the turbulence differences between the sites in Figs. 3 and 4 are real differences of seeing and not due to potential calibration problems or malfunctions of the instruments.

Second, the seeing encountered by TMT at any of the sites would, obviously, be smaller than the seeing measured by the DIMM at 7 m above the ground. This reduces the differences in ground layer strength between the sites, but does not make them equal. Also, at no site is the height of the TMT elevation axis, or even the top of the enclosure, above all of the ground layer for median conditions. A quantitative analysis of this effect is not possible as we do not have sufficient amounts of SODAR data. Semi-quantitative estimates of the magnitude of the effect were presented at several TMT site selection reviews [see, for example, *Schoeck08d*].

Figure 6 shows the median turbulence profiles as calculated from the DIMM and MASS data. The lowest data point of each profile (shown arbitrarily at 250 m) is the ground layer strength calculated from the difference between the DIMM and MASS seeing. The other points are the profiles as measured by the MASS. The plot shows again the stronger ground layer at Mauna Kea 13N and San Pedro Mártir, the stronger high-elevation turbulence of the Chilean sites and the difference in the 16-km layer between Mauna Kea 13N and the other four sites, resulting in the larger isoplanatic angle at Mauna Kea 13N.

The dependence of the DIMM, MASS and ground layer seeing on the wind speed is shown in Fig. 7. The plots on the left use the wind measurements from the weather stations at 2 m above the ground, while the plots on the right use the 7 m sonic anemometer data. The sonic anemometer data are generally more reliable, but cover a shorter period of time (see Table 3). Nevertheless, the general behaviors are the same as a function of both wind speeds. Increases of seeing with wind speed occur at lower AWS wind speeds because the wind at 2 m is generally lower than at 7 m. All sites show an increase of the MASS seeing with wind speed. The ground layer seeing stays flat or decreases for all sites with increasing wind speed before it starts to increase also. The decrease stretches to the highest wind speeds for Tolar and Tolonchar, with a similar behavior for Armazones. Mauna Kea and San Pedro Mártir show a drop or constant value only for the lowest wind speeds before the seeing starts to increase. This behavior, in general terms, is consistent with the difference one can expect between a mountain top site (Tolar, Armazones and Tolonchar) and a site on a plane or plateau (San Pedro Mártir and Mauna Kea 13N). The DIMM seeing behavior is the expected sum of MASS and ground layer seeing.

The dependence of the ground layer seeing on the wind speed is shown again in Fig. 8. Both the ground layer seeing calculated from the DIMM/MASS difference and from the SODAR profiles are shown. Note that the figure shows all data taken at the sites, not only data for times when all instruments were operating simultaneously. Thus, differences between the two curves for each site should be taken with care. The general behavior is, however, very similar for both ground layer measurements at all sites, confirming the trends observed in Fig. 7.

Numerical values for the main site characteristics were extracted from the results reports listed at the beginning of this section and are given in Table 5. Values are medians, unless noted otherwise,

Parameter	Instrument	Tolar	Armazones	Tolonchar	SP Mártir	Mauna Kea 13N
Elevation [m]		2290	3064	4480	2830	4050
Total seeing [as]	DIMM	0.63	0.64	0.64	0.79	0.75
10% DIMM seeing [as]	DIMM	0.42	0.41	0.44	0.50	0.46
Free atmosphere seeing [as]	MASS	0.44	0.43	0.48	0.37	0.33
10% MASS seeing [as]	MASS	0.24	0.23	0.25	0.17	0.15
GL seeing 7 – 500 m [as]	D-M	0.34	0.35	0.32	0.58	0.54
Isoplanatic angle, θ_0 [as]	MASS	1.93	2.04	1.83	2.03	2.69
Coherence time, τ_0 [ms]	M+D	5.2	4.6	5.6	4.2	5.1
Night temperature 2 m [°C]	AWS	14.0	7.5	-0.7	5.4	2.3
Night wind speed 2 m [m/s]	AWS	3.2	6.3	2.7	(2.2)	3.7
Night wind speed 7 m [m/s]	Sonic	4.8	7.2	4.3	(3.3)	5.7
Night humidity 2 m [%]	AWS	19	21	36	38	30
T variation (10 – 90%) [°C]	AWS	5.6	7.5	9.5	16.2	6.8
Clouds: clear fraction	Satellite	87%	89%	82%	83%	76%
Additional weather loss	Combination	1–4%	3–9%	3–8%	2–7%	3–9%
PWV [mm]	Combination	4.0	2.9	1.7	2.6	1.9
Fraction of PWV < 2 mm	Combination	18%	29%	62%	35%	54%

Table 5: Summary of results from the TMT candidate sites. For detailed results see the Results Update Report. All values are medians, unless noted otherwise. For brief descriptions of the quantities presented here see the text in this section, see Section 6 for detailed explanations. The expected uncertainties of the results are given in Section 5. Data that are known to have problems are shown in parentheses.

and describe the following site properties:

Elevation: The site elevation, for reference.

Total seeing, free atmosphere seeing: Integrated seeing from the DIMM and MASS, respectively. Medians and best 10 percentile values are given.

Ground layer (GL) seeing 7 – 500 m: Ground layer seeing calculated from the difference between the DIMM and MASS. The 7.5 – 200 m GL seeing as measured by the SFAS SODAR is not given here because the SODAR data do not cover representative periods for all sites (see Fig. 5).

Isoplanatic angle: Isoplanatic angle, θ_0, obtained from MASS profiles

Turbulence coherence time: Turbulence coherence time, τ_0, obtained from MASS and ground layer τ_0 measurements

Nighttime temperature, wind speed and humidity: Meteorological values obtained at 2 m above the ground with the weather stations and at 7 m with the sonic anemometer

Temperature variations (10 – 90%): Difference between the ninetieth and tenth percentile of the temperature distributions measured at 2 m above the ground, thus giving the temperature range not exceeded 80% of the time

Cloud cover, clear fraction: Fraction of time without clouds, obtained from satellite data

Additional weather loss: Fraction of time that is lost due to weather factors other than clouds. These numbers are based on very specific assumptions that might not be true for TMT during operations. Only ranges of numbers can therefore be given here. See *Schoeck08b* for details.

PWV and fraction of PWV < 2 mm: Median PWV value and fraction of time the PWV is below 2mm, obtained from a combination of satellite and ground data

7.3 Site Merit Function

In order to understand the science potential of each candidate site better, TMT has developed a metric by which we can compare the sites. This Site Merit Function is described in a separate document [*Nelson08*] which is provided together with this report. It also contains the results from applying the metric to the site data.

8 Supplementary Documents

The following documents containing background information are available together with this report. Unless noted otherwise, these documents are available in the same DocuShare folder as this document.

Reports describing results from the candidate sites:

- *Els08a*: Sebastian Els et al., **TMT Site Selection Results Update**, TMT internal report (2005 – 2008)
- *Els08b*: Sebastian Els et al., **Report on the meteorological conditions up to 30 m above Cerro Armazones, Cerro Tolonchar and San Pedro Mártir**, TMT internal report (2006 – 2008)
- *Nelson08*: Jerry Nelson, **TMT Site Merit Function**, TMT internal report (2008)
- **Satellite Data Analysis reports**: DCC Site Selection folders, Collection 1129, in particular:
  - *Erasmus03*: D. André Erasmus and C.A. van Staden, **A Comparison of Satellite-Observed Cloud Cover and Water Vapor At Mauna Kea and Selected Sites In Northern Chile, the Southwestern U.S.A. and Northern Mexico**, study for the AURA New Initiatives Office (2003)
  - *Ivanescu07a*: Liviu Ivănescu, Rupert A. Spann, D. André Erasmus, **Satellite Study for TMT**, TMT internal report (2007)
  - *Ivanescu07b*: Liviu Ivănescu, Rupert A. Spann, D. André Erasmus, **Climate Study for TMT**, TMT internal report (2007)
- **Computational Fluid Dynamics (CFD) simulation reports**: DCC Systems Engineering folders, Collection 1172

Requirements documents:

- *SiRD*: **Site Selection Requirements and Strategy Document**
- *SRD*: **Science-Based Requirements Document**: DCC Project Science folders
- *ORD*: **Observatory Requirements Document**: DCC Systems Engineering folders

Documents describing instruments, methods or calibration results:

- *Britton06*: Matthew Britton, **The Anisoplanatic Point Spread Function in Adaptive Optics**, PASP 118, 885 (2006)
- *Chun06*: Mark Chun, Bob McLaren and Rolf-Peter Kudritzki, **Seeing at 13N** and comments by the TMT Project, Institute for Astronomy report (2006)
- *Els06a*: Sebastian Els and Matthias Schöck, **Dependence of MASS results on the instrument characterization – a sensitivity study**, TMT internal report (2006)
- *Els06b*: Sebastian Els, **Sensitivity of MASS results on the spectral response functions**, TMT internal report (2006)

- *Els06c*: Sebastian Els and David Walker, **Impact of air traffic on the potential sites for TMT in Chile**, TMT internal report (2006)
- *Els07c*: Sebastian Els and Matthias Schöck, **Impact of vignetting of the MASS device on the turbulence resuls**, TMT internal report (2007)
- *Els07d*: Sebastian Els and Konstantinos Vogiatzis, **Revealing the onset of free convection in terrestial planet atmospheres**, IAU Symp. 239, (2007)
- *Els07e*: Sebastian Els and Matthias Schöck, **Side by side comparison of two MASS devices - results of the Tololo campaign**, TMT internal report (2007)
- *Els08c*: Sebastian Els et al., **Study on the precision of the MASS turbulence profiler employed in the site testing campaign for the Thirty Meter Telescope**, accepted for publication in Applied Optics (2008).
- *Els08d*: Sebastian Els et al., **The Multi Aperture Scintillation Sensor (MASS) used in the site selection of the Thirty Meter Telescope (TMT)**, Proc. SPIE (2008)
- *Kornilov03*: Victor Kornilov et al., **MASS: a monitor of the vertical turbulence distribution**, Proc. SPIE 4839, 837–845 (2003)
- *Kornilov05*: Victor Kornilov and Nicolai Shatsky, **MASS data reprocessing**, Sternberg Astronomical Institute report (2005)
- *Lopez93*: Bruno Lopez and Marc Sarazin, **The ESO atmospheric temporal coherence monitor dedicated to high angular resolution imaging**, Astronomy and Astrophysics 276, 320–326 (1993)
- *Oncley04*: Steve Oncley and Tom Horst, **Calculation of C_n^2 for visible light and sound from CSAT3 sonic anemometer measurements**, NCAR/ATD report (2004)
- *Otárola08*: Angel Otárola et al., **Statistical Characterization of Precipitable Water Vapor at San Pedro Martir Sierra in Baja California**, TMT internal report (2008)
- *Racine06a*: René Racine, **A Comparison of Astronomical Seeing at the Ridge and 13N Mauna Kea Sites**, TMT internal report (2006)
- *Racine06b*: René Racine, **The Statistics and Probable Cause of the Differences in Simultaneous Seeing Values between the Mauna Kea 13N and UH 2.2 m Telescope Sites**, TMT internal report (2006)
- *Riddle06*: Reed Riddle, **Calibration of the dust sensors used in the site testing program**, TMT internal report (2006)
- *Riddle07a*: Reed Riddle et al., **TMT Site Testing: Tolonchar 30 m Tower Installation and Calibration**, TMT internal report (2007)
- *Riddle08*: Reed L. Riddle et al., **An Analysis of Light Pollution at the Thirty Meter Telescope Candidate Sites**, Proc. SPIE (2008)
- *Sarazin90*: Marc Sarazin and François Roddier, **The ESO differential image motion monitor**, Astronomy and Astrophysics 227, 294–300 (1990)

- *Schöck06*: Matthias Schöck, **Mauna Kea 13N - Summit Ridge Comparison**, presentation to the TMT Project (2006)
- *Schöck07a*: Matthias Schöck, **Note on an Investigation of TMT Site Selection DIMM Strehl Ratios and DIMM Telescope Vibrations**, presentation to the TMT Project (2007)
- *Schöck07b*: Matthias Schöck, **Note on the Comparison of Several DIMMs at San Pedro Mártir**, TMT internal report (2007)
- *Schöck07c*: Matthias Schöck, **Comparison of DIMM and MASS Results at Cerros Armazones and Paranal**, presentation to the TMT Project (2007)
- *Schöck08a*: Matthias Schöck, Tony Travouillon and Angel Otárola, **Precipitable Water Vapor Data Used in TMT Site Selection**, presentation to the TMT Project (2008)
- *Schöck08b*: Matthias Schöck and Warren Skidmore, **TMT Site Selection Cloud Cover and Usable Time Analysis**, presentation to the TMT Project (2008)
- *Schöck08c*: Matthias Schöck and Reed Riddle, **TMT Site Selection Light Pollution Analysis**, presentation to the TMT Project (2008)
- *Schöck08d*: Matthias Schöck, **TMT Site Selection Update**, 15 January 2008 site selection review presentation to the TMT Project (2008)
- *Skidmore06a*: Warren Skidmore, **Cross calibration of the CSAT3 sonic anemometer and automatic weather station - reports and plans**, TMT internal report (2006)
- *Skidmore06b*: Warren Skidmore et al., **Evaluation of sonic anemometers as highly sensitive optical turbulence measuring devices for the Thirty Meter Telescope site testing campaign**, Proc. SPIE 6267, 64 (2006)
- *Skidmore07a*: Warren Skidmore et al., **Report of the calibration of the T2-Armazones 28m tower air temperature sensors and sonic anemometers, the cross comparison of weather stations and sonic anemometers and the turbulence measurements of sonic anemometers and newire thermocouples**, TMT internal report (2007)
- *Skidmore07b*: Warren Skidmore and Sebastian Els, **Investigation of the quality of wind speed and direction measurements from the Monitor Sensor AWS and the effect of air density on measured wind speed**, TMT internal report (2007)
- *Skidmore08a*: Warren Skidmore and Matthias Schöck, **Manual assessment of the cloud coverage from TMT site testing ASCA observations**, TMT manual (2008)
- *Skidmore08b*: Warren Skidmore et al., **Using All Sky Cameras to determine cloud statistics for the Thirty Meter Telescope candidate sites**, Proc. SPIE (2008)
- *Socas-Novarro05*: H. Socas-Novarro et al., **Solar Site Survey for the ATST I: Analysis of the Seeing Data**, PASP 117, 1296–1305 (2005)
- *Steinbring06*: Eric Steinbring, **Mauna Kea Sky Transparency from CFHT SkyProbe Data**, TMT internal report (2006)

- *Tokovinin06a*: Andrei Tokovinin, **MASS simulations under strong scintillation**, CTIO report (2006a)
- *Tokovinin06b*: Andrei Tokovinin, **Calibration of the MASS time constant measurements**, CTIO report (2006b)
- *Travouillon07*: Tony Travouillon, **SODAR calibration and comparison report**, TMT internal report (2007)
- *Travouillon08a*: Tony Travouillon, **A comparison of the MASS coherence time with radiosonde profiles and NCEP reanalysis**, TMT internal report (2008)
- *Travouillon08b*: Tony Travouillon et al., **Temporal Variability of the seeing at the TMT candidate sites**, Proc. SPIE (2008)
- *Travouillon08c*: Tony Travouillon, Sebastian Els and Matthias Schöck, **Temporal analysis of the seeing**, TMT internal report (2008)
- *vanDam06*: Marcos van Dam et al., **Angular anisoplanatic error in laser guide star adaptive optics**, Proc. SPIE 6272 (2006)
- *Walker06*: David Walker et al., **Monitoring the night sky with the Cerro Tololo All-Sky camera for the TMT and LSST projects**, Proc. SPIE 6267 (2006)
- *Wang07*: Lianqi Wang et al., **High Accuracy DIMM Measurements for the TMT Site Testing Program**, Appl. Opt. 46, 6460–6468 (2007)